PhD Thesis

Title

NMR study of structure-activity relationship of the biologically active peptide Humanin and the membrane binding protein CERT

August 2016,

Department of Biological Science

NESREEN IBRAHIM ALSANOUSI MOHAMMED

Graduate School of Science Osaka University

NMR study of structure-activity relationship of the biologically active peptide Humanin and the membrane binding protein CERT

By

Nesreen Ibrahim Alsanousi Mohammed

Supervised by

Prof. Toshimichi FUJIWARA

Institute for Protein Research, Osaka University

Table of contents

Table of contents……..…….ii

Abbreviations……..v

Abstract…….……..…vi

Part I: NMR Study of Structure – Activity relationship of Humanin

1 Introduction and Aims…….…….1

1.1 Mitochondrial-derived bioactive peptides…….……1

1.2 Humanin……..…..2

1.2.1 The discovery of Humanin……..……..2

1.2.2 Protective effects of Humanin and analogues……...3

1.2.3 Mechanism of action of Humanin…….4

1.2.4 Humanin structure –function relationship…….6

1.2.5 Structural studies of humanin peptide and analogs……...7

1.3 Alzheimer's diseases and the amyloid-beta peptide (Aβ)……..…9

1.3.1 Alzheimer's diseases (AD)……..…9

1.3.2 Amyloid β peptide…….....9

1.3.3 Metal ions in AD…….11

1.4 Structural studies by solution NMR spectroscopy……..12

1.5 Using NMR techniques for characterization of ligand binding……..14

1.6 Objectives and significance of the study…….16

2 Experimental……...17

2.1 Sample preparation……..17

2.2 Circular dichroism measurements……17

2.3 Transmission electron microscopy……...17

2.4 NMR spectroscopy……...18

2.5 Solution structure determination of HN D-Ser……19

2.6 Determination of the amyloid β-binding site of HN D-Ser14…….20

2.7 Determination of zinc ion binding site on the HN D-Ser14 variant……20

3. Results……21

3.1. Aβ40 secondary structure analysis by CD spectroscopy……21

3.2 Inhibition of amyloid-β fibrillation by HN wild-type, HN S14G, and HN D-Ser14 observed by TEM……22

3.3 Determination of solution structure of the HN D-Ser14 variant……..23

3.4 Oligomeric state of the HN D-Ser14 variant……27

3.5 Structural comparison between HN wild-type, HN S14G, and HN D-Ser14……..28

3.6 Amyloid β-binding site of HN D-Ser14……...30

3.7 Identification of zinc ion binding site on the HN D-Ser14 variant……..33

4. Discussion……35

4.1 Structural modulation of Aβ by HN D-Ser14……..35

4.2 Structural impact of D-isomerization of HN……35

4.3 Aβ recognition by HNs……37

4.4 Zinc ion binding to HN D-Ser14……..38

4.5 Electrostatic potential of HNs surface……..41

5 Concluding remarks……43

Refrences……...……..45

Part II. Solution NMR studies of CERT-PH domain……50

1 Introduction and Aims……50

1.1 Lipid transport by lipid transfer proteins……50

1.2 Ceramide Trafficking Protein (CERT)……51

1.3 Phospholipid bilayer Nanodisc……55

1.4 Study of protein lipid binging using ITC……56

2 Experimental……...58

2.1 Expression and purification of CERT PH domain……...58

2.2 Preparation of Nanodisc……...58

2.3 NMR measurements……59

2.4 ITC experiments……...60

3 Results and discussion…….....61

3.1 CERT PH binding to PI4P-containing nanodisc……..61

3.2 Membrane binding site on CERT PH domain…….62

3.3 Characterization of CERT PH domain binding to lipid bilayer with ITC……...……64

4 Conclusions……..66

References…….…..67

Acknowledgements……69

Appendix……70

Abbreviations

HN	Humanin
HNG	Ser14Gly mutant of Humanin
HN D-Ser14	Humanin variant containing D-form Ser14 residue
AD	Alzheimer's disease
Aβ	Amyloid-β
$A\beta_{42}$	42 amino acid form of amyloid-β
TFE	2,2,2-trifluoroethanol
Bax	Bcl-2-associated X
IGFBP-3	Insulin-like growth factor-binding protein-3
GH/IGF axis	Growth hormone/insulin-like growth factor-1
FPRL1	Formyl peptide receptor-like 1
CNTFR	Ciliary neurotrophic factor receptor
ROS	Reactive oxygen species
MDPs	Mitochonderial-derived peptides

Abstract

Humanin, a bioactive peptide consisting of 24 amino acid residues, was isolated from brain tissues of patients of Alzheimer's diseases. It has been reported that Humanin significantly suppresses various aging-related cell death that caused by amyloid fibrils aggregates and oxidative stress. Previous literature suggested that the cytoprotective activity of humanin peptide was remarkably enhanced by optical isomerization of the Ser14 residue from L- to D-form as post-translational modification. As a result, Humanin D-Ser14 variant can significantly inhibit cell death with extremely low concentration, and thereby it is considered that Humanin is promising molecules in an effort to develop new drugs against aging-related cell degenerative diseases such as AD. However, molecular mechanisms of enhancement of the cytoprotective activity of Humanin caused by D-isomerization of the specific serine residue are remains unclear.

Humanin D-Ser14 exhibited potent inhibitory activity against fibrillation of amyloid-β and remarkably higher binding affinity for amyloid-β than that of the Humanin wild-type and S14G mutant. In addition, we determined the solution structure of Humanin D-Ser14 by nuclear magnetic resonance (NMR) and showed that D-isomerization of the Ser14 residue enables drastic conformational rearrangement of Humanin. Furthermore, we identified an amyloid-β-binding site on Humanin D-Ser14 at atomic resolution by NMR. These biophysical and high-resolution structural analyses clearly revealed structure–function relationships of Humanin and explained the driving force of the drastic conformational change and molecular basis of the potent anti-amyloid-β fibrillation activity of Humanin caused by D-isomerization of the Ser14 residue. This work has shown the correlations between the functional activity, tertiary structure, and partner recognition mode of Humanin and can lead to elucidation of the molecular mechanisms of the cytoprotective activity of Humanin. Furthermore, it is considered that interactions of Humanin with amyloid-beta and zinc ion have an important consequence for pathogenesis or development of AD. However, detail of the zinc ion recognition mode of the Humanin has not been clarified. We identified zinc ion binding site on the Humanin with atomic resolution.

The second part of the thesis shows a study of the mechanism of CERT-PH domain biding to Golgi-membrane. Ceramide transfer protein (CERT) mediates ER-to Golgi trafficking of ceramide. CERT consists of two main functional domains, the plecksterin homology domain (PH), which serves to target the Golgi apparatus, and the START domain, capable of catalyzing inter-membrane transfer of ceramide. CERT-PH specifically binds phosphatidylinositol 4-phosphate (PI4P). In this work PI4P incorporated phospholipid bilayer nanodisc were prepared to assess the PH-domain–PI4P interaction on the Golgi membrane by solution NMR techniques.

The mechanism of binding and the biding site of CERT PH on the phospholipid bilayer were identified by NMR. The NMR study revealed that Trp residues in CERT-PH interacted with the lipid head groups in the membrane and the neighboring basic (4 Arg and 2 Lys) residues should interact specifically with the anionic head group of PI4P. This derives the CERT PH domain to PI4P recognition and localization on the membrane. Iisothermal titration calorimetry (ITC) technique were used to gain insights into the thermodynamic signatures of the interaction, the result revealed that CERT PH domain binds to PI4P containing membranes with a high affinity with stoichiometry 1:1. This binding mode confers the function of the Golgi selective recognition on the PH domain of CERT.

Publication

Nesreen Alsanousi, Toshihiko Sugiki, Kyoko Furuita, Masatomo So, Young-Ho Lee, Toshimichi Fujiwara, and Chojiro Kojima

"Solution NMR structure and inhibitory effect against amyloid-β fibrillation of Humanin containing a D-isomerized serine residue"

Biochemical and Biophysical Research Communications, in press (2016)

NMR Study of Structure – Activity relationship of the biologically active peptide Humanin

1 Introduction

1.1 Mitochondrial-derived bioactive peptides

Mitochondria, a unique intracellular organelle that contain their own genome, responsible for several pivotal cellular activities ranging from energy production, regulation of programmed cell death (apoptosis), generation of reactive oxygen species (ROS), regulation of cellular levels of metabolites, heme synthesis, calcium homeostasis and many other cellular functions [1]. Mitochondrial-derived peptides (MDPs) are a class of small peptides that are encoded within the mitochondrial genome. These class of peptides can be considered as a retrograde signaling molecules provides communication by the mitochondria to regulate cellular processes [2, 3]. The discovery and use of these biologically active peptides can contribute to the understanding of many important mechanisms inside the cell, and hence the understanding of disease origin. For example the multifunctional peptide humanin; that is encoded within 16S ribosomal RNA gene in the mtDNA. Humanin peptide was discovered by three labs independently when screening for proteins that may involve in Alzheimer's diseases, apoptosis, and signaling of IGF-1 [4,5,6] and more recently a new mitochondrial derived peptide was discovered, MOTS-c peptide, which is also have useful properties in regulating gene expression and cellular metabolism as indicated by its effects on insulin resistance and obesity [7].

Therefore, the study of this important class of peptides will expand our understanding of the role that played with the mitochondrial derived peptides in

intracellular signaling throughout the body to regulate various activities like cell survival and metabolism. Moreover, this class of biologically active peptides can be optimized into drug candidates, for treatments of age-related diseases.

1.2 Humanin

1.2.1 The discovery of Humanin

Humanin is a novel mitochondrial-associated peptide discovered in 2001 by Hashimoto *et al*. while screening cDNA library constructed from occipital lobe of the brain tissue of Alzheimer's disease (AD) patient. After its discovery, humanin peptide have been found in other tissues including, heart, liver, skeletal muscle, colon, kidney, tests, hypothalamus and vascular wall. Humanin peptide contains 24 amino acids (MAPRGFSCLLLLTSEIDLPVKRRA), encoded from a small open reading frame (ORF) in the mitochondrial genome (mtDNA) within the 16S RNA coding region [4, figure 1]. And it is believed to be the first newly discovered peptide that derived from the mitochondria. The length of functional HN would differ according to the site of translation, in the cytoplasm of human cells humanin mRNA is translated to a 24-amino acid peptide but to 21-amino acid peptide instead in the mitochondria [8].

Humanin has also been cloned as a Bcl-2-associated x protein (BAX) partner that could prevent the BAX-dependent apoptosis in the cells [5]. Humanin also discovered by Ikonen *et al*. (2003) as a binding partner to IGFBP3, where it can block the IGFBP-induced epoptoic effects to the glial cells [6].

1.2.2 Protective effects of Humanin and analogues

The HN peptide exhibits powerful inhibition activity against neuronal cell death caused by insult of broad spectrum of familial Alzheimer`s diseases (AD). Recently, it have been reported that HN shows significant cytoprotective effect not only against AD-related neuronal cell death but also against various types of inflammation and cell damages caused by oxidative stress, hyperglycemia, and ischemia [3,9,10]. The protective effects of HNs have been proved by several studies *in vitro* and *in vivo*. To date, Humanin and its potent analogues have been shown to play a role in multiple diseases including cardiovascular disease, memory loss, type 2 diabetes and stroke. And the mechanism that common to all of these age-related diseases is oxidative stress and mitochondrial dysfunction [11].

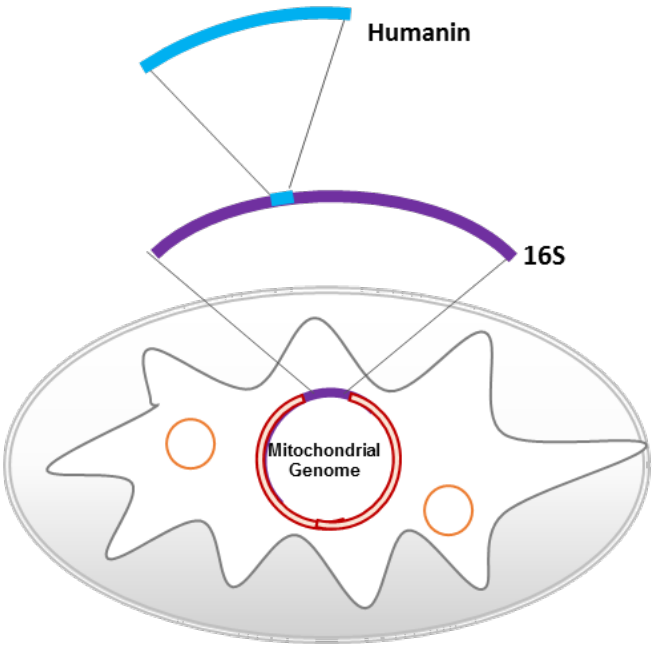

Figure 1: The Humanin gene. It is found within the 16S rRNA in the mtDNA.

1.2.3 Mechanism of action of Humanin

Humanin peptide is proven to be secreted and acts extracellularly following the translation of humanin gene. The cytoprotective activity of humanin peptide is appears to be mediated by interactions with intracellular counterpart molecules [5,6,12] or cell membrane-surface receptors in an autocrine manner [3,413,14]. In cytoplasm, HN binds to Bax (Bcl-2-associated X) protein, which plays a central role in pro-apoptotic regulation on the mitochondria by releasing cytochrome c into the cytoplasm, and antagonizes activation of the Bax resulting inhibition of cell death [5].

It was also reported that HN interacts with IGFBP-3 (Insulin-like growth factor-binding protein-3), which regulates function of insulin-like growth factor (IGF) and also induces cell death independently of the action of IGF, and antagonizes its apoptosis induction activity [6].

In addition, it was reported that FPRL1 (formyl peptide receptor-like 1), a seven-transmembrane G-protein coupled receptor (GPCR), serves as cell-surface receptor of HN. Interaction between FPRL1 and HN activates ERK1/2, and it leads anti-inflammatory and cytoprotection actions. Interestingly, although the FPRL1 also participate in recognition of $A\beta_{42}$ and its interaction causes cytotoxic action, its activity was reversed in the presence of HN. It suggests that HN binds to the FPRL1 in direct competition with $A\beta_{42}$, or HN binds to FPRL1-interaction site of $A\beta_{42}$ [15].

Furthermore, it has been previously reported that a heterotrimeric complex of transmembrane proteins CNTFR/WSX-1/gp130 plays a role as a cell-surface receptor of HN and activates STAT3 signal transduction [13]. Other proteins also can bind to humanin

and affect its activity and expression; TRIM11 binds and destabilize humanin [16] and VSTM2L binds to humanin and inhibit its activity [17, figure 2].

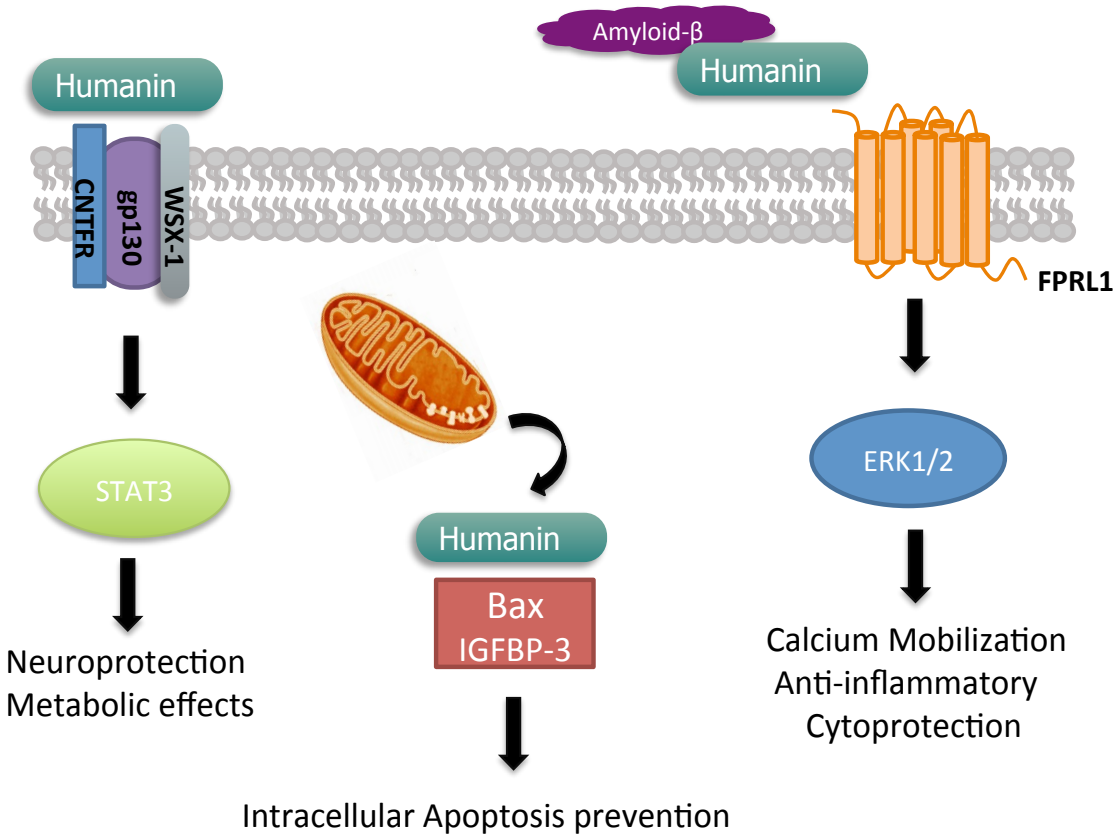

Figure 2.Cellular actions of Humanin peptide through interaction with binding partners. Adopted from [3]. Intracellular humanin interacts with proteins such as Bax and IGFBP-3 and prevent epoptosis. Extracellular humanin acts through two types of cell membrane receptors to regulates important cellular processes such as inflamation, metabolism, and cell suvival, a trimeric receptor involving CNTFR/WSX-1/gp130, which relays signals through the STAT3 signaling pathway, and the formyl-peptide receptor-like-1 (FPRL1), which relays signals through the ERK 1/2 signaling pathway.

1.2.4 Humanin structure –function relationship

Molecular studies on the humanin family have revealed that there is a strong relation between the humanin peptides function and structure. Figure 3 shows the structure of Humanin peptide and the important residue that necessary for its action. The complete sequence of humanin may function as signal peptide [21]. Known humanin analogues have been classified by Arakawa et al. [67] into 6 groups [Table 1]. In this classification, L9R-HN come with class 1 and is characterized by the lack of its ability to be secreted, HNG, class 2 analog, in which Ser14 mutated to Gly or D-Ser. HNA and S7A-HN are belong to class 3 and are considered inactive mutants. The HN active analog AGAC8R-HNG17, comprise class 4. Class 5 contains the HN analog EF-S7A-HN was shown to restore the inactive HN mutant. Class 6 is Colivelin, it is another HN analog which was synthesized to promote the chemical and biological stability of HN peptide. [67].

HN peptide	MAPRGFSCLLLLTSEIDLPVKRRA
Essential residues	
Dimerization	------S-L---------------
Secretion	--------LLL------------
Neuroprotection	--P---SCL--LTS----P-----

Figure3. Structure of Humanin peptide and the residues essential for its function [21].

Table 1. Classification of Humanin peptide analogues [67].

Class	Peptide name	Mutation
	HN	MAPRGFSCLLLLTSEIDLPVKRRA
Class 1	L9R-HN	Leu 9 ⟶ Arg
Class 2	HNG	Ser 14 ⟶ Gly
Class 2	D-Ser 14	L-Ser 14 ⟶ D-Ser
Class 3	HNA	Cys 8 ⟶ Ala
Class 3	S7A-HN	Ser 7 ⟶ Ala
Class 4	AGA-HNG	Arg 4 ⟶ Alan, Phe 6 ⟶ Ala, Ser 14 ⟶ Gly
Class 4	AGAC8R-HNG17	Deletion of N-terminal MA Arg 4 ⟶ Ala, Phe 6 ⟶ Ala Cys 8 ⟶ Arg, Ser 14 ⟶ Gly Deletion of c-terminal VKRRA
Class 5	EF-S7A-HN	Ser 7 ⟶ Ala N-terminal addition of EFLIVIKS
Class 6	Colivelin	ADNF9-AGAC8R-HNG17

1.2.5 Structural studies of humanin peptide and analogs

Tertiary structures of HN wild type were previously investigated by solution NMR techniques. It was demonstrated that although HN forms predominantly unstructured conformation in an aqueous solution [18,19], in the presence of TFE, which mimic lipophilic environment such as lipid membranes or hydrophobic interaction site on binding partners, the HN forms significant helical structures [18-20]. It has been considered that the HN exists in a cytoplasm or extracellular solely, and the large moiety of the HN predominantly unstructured. However, it acquires helical conformation when it found and interacts with functional partners. Therefore, it is appropriate that the solution structures of HN determined in such a lipophilic environment is regarded as highly close to the "active

form" to exert cytoprotection activity.

HN has a central hydrophobic (from Gly5 to Leu18, GFSCLLLLTSEIDL) and positively charged C-terminal (from Pro19 to Ala24, PVKRRA) regions. Previous studies have revealed that the Pro3-Pro19 region in the HN sequence plays central role in its cytoprotective activity [21]. In the region, by performing alanine-scanning mutagenesis assay, it was demonstrated that the Pro3, Cys8, Leu9, Leu12, Thr13, Ser14 and Pro19 are essential residues to exert its cytoprotective action [22]. However, it is not elucidated how these residues operate cytoprotection action of HN.

Incidentally, it was also reported that substitution of Ser14 of the HN to glycine residue (HNG) significantly enhances its cytoprotective activity by 1000-fold comparing to parent HN [4, 23]. Interestingly, optical isomerization of Ser14 residue from L- to D-form also resulted in 1000-fold enhancement of HN-mediated cytoprotection [24]. Solution structures of HNG demonstrated that originally helix structure of carboxyl terminal region from the Gly14 to Ala24 was clearly disordered [19]. Although it is assumed that increasing flexibility or changing its conformation around the Ser14 or carboxyl terminal region from the Ser14 caused by substitution of the Ser14 residue influences intensity of its cytoprotection activity, however, tertiary structure of the HN D-Ser14 variant have not been determined and therefore molecular mechanisms of which D-isomerization of the Ser14 residue leads drastic augmentation of cytoprotective activity of HN are remain unknown.

It is well known that D-isomerization of serine or aspartic acid residues is one of the post-translational modifications of polypeptides and it plays important role in modulation of physical properties or biological functions of the polypeptides [25]. Therefore, it is highly probable that HN D-Ser14 variant is generated in living tissues and is

working as inherent powerful cellular guardian [24].

1.3 Alzheimer's diseases and the amyloid-β peptide (Aβ)

1.3.1 Alzheimer's diseases (AD)

Alzheimer's (AD) is a progressive neurodegenerative disease that causes a progressive loss of mental capacity among the aging populations. AD is the most common cause of the type of dementia that belongs to the group of neurodegenerative disorder diseases. The symptoms of AD was first assigned at 1907 by Alois Alzheimer who was a psychiatrist and neuropathologist [26]. Age is the major risk factor in developing Alzheimer's, although this disease is not a normal part of the aging process. AD causes neuronal damages that cause the features of dementia patients such as general confusion, depression and loss of memory. Alzheimer's disease (AD) is defined by two pathological hallmarks; the formation and accumulation of amyloid plaques and neurofibrillar tangles in the brain [27, 28].

Up to date, research has expose a great progress about Alzheimer's, but, much is yet to be discovered about the precise biological changes that responsible for Alzheimer's, and how this disease could be prevented or treated.

1.3.2 Amyloid β peptide

The aggregation of amyloid β peptide is closely linked to the pathogenesis of Alzheimers disease [29]. Based on extensive studies, it has been determined that the primary constitute of the amyloid plaques is an aggregates of a small peptide called the amyloid β peptide (Aβ), which was first isolated in 1984 [30], and the neurofibrillar

tangles is consist of aggregated tau protein mainly. The molecular mass of Aβ is about 4.3 kDa and consists of 38-43 residues with the two most common forms $A\beta_{40}$ (1-40) and $A\beta_{42}$ (1-42) [figure 4]. The aggregation process of Aβ peptides in the brain, which derived by misfolding, is one of the main causes of AD [31]. The 40-residue peptide Aβ (1–40) is the most abundant Aβ forms in normal and AD brains, followed by the 42-AA residue peptide. The $A\beta_{42}$ peptide with 42 amino acids has been shown to be highly susceptible to aggregation and toxic behavior among all the Aβ peptides [32-34]. The aggregation process of Aβ peptides leads to formation of polymorphic oligomers, protofibrils, and fibrils, which individually cause toxic effects to the cells. Amyloid fibrils are a fibrillar polypeptide aggregates that consist of a cross-β structure. On the past, Aβ fibrils were considered the neurotoxic form and causative agent of AD, whereas in the last two decade further investigations suggested that the most toxic form of Aβ is the oligomers causing oxidative stress, interacting with signaling receptors, disturbing metal homeostasis and disrupting neuronal cell membrane [35]. Membrane disruption is one of the major pathways of toxicity induced by Aβ oligomers [36].

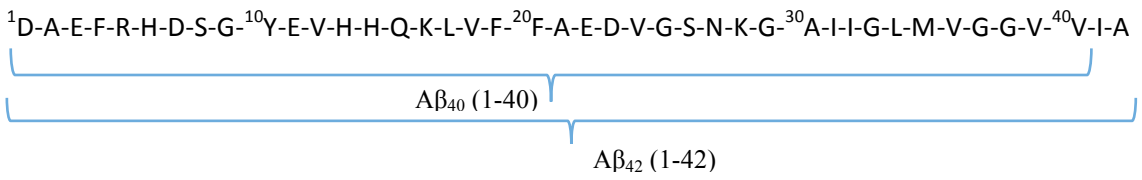

Figure 4. Sequences of $A\beta_{40}$ and $A\beta_{42}$

1.3.3 Metal ions in AD

AD patient's brain characterized by impaired metal homeostasis and metal ions have been proposed to play a key role in AD pathogenesis [37]. Several studies have revealed that in AD disease, copper, zinc, and iron homeostasis may perturbed and could underlie an increased oxidative stress [38]. In the AD brain, metal ions are found co-localized with Aβ. Metal ions have been shown to bind to Aβ and modulate its aggregation process in vivo and in vitro [39]. In the brain, zinc, copper and iron ions concentration is higher compared to the other body parts [40]. In AD patients' brain, excess of metal ions was reported in amyloid plaques compared to the surrounding tissue [38]. Zinc and copper ions were found with a heterogeneous distribution in amyloid plaques, and, with increased presence in the regions that contains a high β-sheet content [41].

Zinc ions are the most abundant trace metal in the brain tissue, and AD is characterized by accumulation of zinc ion in cerebral Aβ deposits [42.43]. There are many evidences suggesting ionic zinc is able to accelerate the aggregation of Aβ, and actually, metal chelation has been reported as one of the efficacious therapy against AD [43]. Recently, it was reported that HN also bind to zinc ion and have a suppressive influence to aggregation or fibrillation of Aβ promoted by binding to zinc ion [44]. However, zinc ion binding site on the HN and their interaction mode are unknown, and therefore the molecular mechanism how HN influences aggregation of Aβ and Aβ-zinc ion interaction are remain unclear. In an effort to prevent or control development of diseases, which caused by cell death derived from oxidative stress, inflammation, or failure of proliferation signal transduction, including such as AD, prevention of cell death is one of the important and reasonable strategies. Therefore, investigation of molecular mechanisms of

cytoprotective activity of HN would beneficial to develop powerful new anti-AD and cytoprotective drugs based on the character of HN and insights of molecular mechanisms of HN-mediated cytoprotection.

1.4 Structural studies by solution NMR spectroscopy

For understanding the function of biological macromolecules, the 3D structure is needed. Solution NMR spectroscopy enables the determination of 3D structures of proteins in solution under optimized conditions, near to the physiological conditions of the macromolecule. The knowledge of molecule structure in solution is important; the solution conditions can be adjusted. Solution NMR applications can also include the study of the dynamics of the molecular structure, and also the structural, dynamic and kinetics of the interaction between proteins or proteins with other molecules.

Resonance assignment

The resonance assignment of the macromolecule is required for structural and dynamic studies by NMR. A sequential procedure can be used to assign resonances of peptides and proteins [45]. For small un-labeled proteins and peptides, ^{1}H signals can be assigned by the 2D homonuclear experiments; correlation spectroscopy (COSY) and Total correlation spectroscopy (TOCSY), in order to identify the spin systems and Nuclear Overhauser Effect Spectroscopy (NOESY), used for sequentially connecting the residues.

2D COSY (correlation spectroscopy)

COSY was the first NMR experiment, described in 1971. Homoneclear experiment used for analyzing proton spectra. From COSY spectrum you can identify the chemical shift of

spins that are coupled to one another via scalar coupling, this enables to follow the *J*-coupling connectivities in the molecule (Fig 5). The COSY experiment is almost exclusively used for small (non-labeled) peptides. [46]

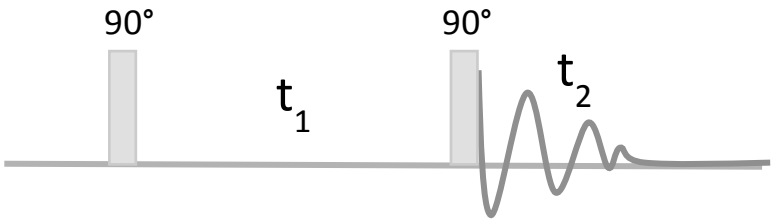

Figure 5. A pulse sequence of a standard COSY. Consist of a single RF pulse followed by a specific evolution time (t_1) followed by a second pulse and finally a measurement period (t_2).

2D TOCSY (Total Correlation Spectroscopy)

In the 2D ^{1}H-^{1}H TOCSY experiment cross peaks of coupled protons are observed (^{1}H-^{1}H coupling). The magnetization is transferred during a multi-pulse spin-lock period along the spin system as long as protons are scalar coupled. Interactions depend on the spin-lock strength, about 12 kHz typically. J-couplings do not maximize with the field strength, but chemical shifts do. All the couplings during a spinlock period are strong: The strong coupling lead to efficient mixing of all the protons in a coupled spin system. Therefore, it is useful to identify the larger interconnected networks of spin couplings. The key part of the experiment is the period of isotropic mixing. The TOCSY mixing time can be varied between 15 to 100 ms with shorter values giving a COSY-like spectrum and longer values giving complete spin-systems figure 6 shows the pulse sequence for TOCSY. [46]

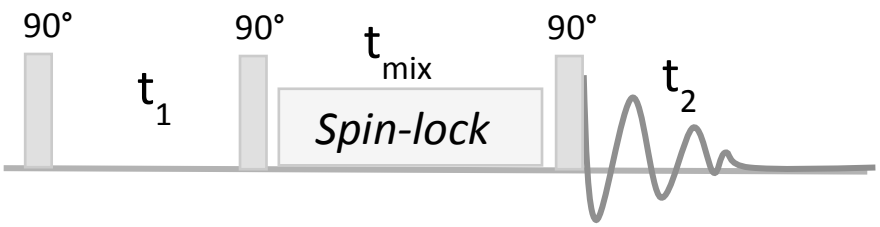

Figure 6. A pulse sequence of the TOCSY experiment. The period of the isotropic mixing (t_{mix}) is the key part of the experiment.

2D NOESY (Nuclear Overhauser effect Spectroscopy)

The NOESY experiment is necessary for the determination of protein structure. NOESY experiment uses the dipolar interaction of spins, the nuclear Overhauser effect (NOE), to correlate protons. In NOESY experiment, the direct dipolar couplings provide the principal means of cross-relaxation, and so spins which are close to one another in space are those that undergoes cross-relaxation. NOESY allow us to identify witch nuclei are close in space (within 5 to 6Å), Thus providing complementary information to scalar coupling, which relates to the bonding network. The sign of the NOE depends on the magnitude of the rotational correlation time and hence the molecular weight. [46]

1.5 Using NMR techniques for characterization of ligand binding

The chemical shifts are very sensitive to the change in the environment; therefore, chemical shift perturbation (CSP) or chemical shift mapping is the straightforward technique to study the binding of a ligand to a protein or a peptide. Perturbations in the chemical shifts can be caused by change in the covalent molecular structure, and or the non-covalent interactions with other molecules or binding partner. The location of the ligand binding is determined on the bases of shift changes. There are several aspects of

protein-ligand interactions that can be characterized by NMR; determination of the binding affinity, location of the ligand binding site on the protein, and possibly the structure of the protein-ligand complex [47, 48].

^{15}N HSQC titration for Chemical shift perturbation (CSP):

For determining the location of the bound ligand, the ligand is titrated into the protein and the changes in the chemical shift is recorded at each step of titration by measuring 2D ^{15}N-HSQC spectra. From the same measurements we can determine the ligand-binding site and also we can calculate the Kd value. CSP technique can be useful even without the chemical shift assignment of HSQC spectra, it is therefore very useful in drug discovery. One big advantage of the CSP method is that it is not necessary to calculate the NMR structure, we can use the available crystal structure and map the chemical shifts change onto it. The binding of the ligands to their target moleculoes lead to changes in the chemical shifts. Changes in the chemical shifts is because of the alteration on the electron densities, this could be due to a direct effect of the ligand binding or can be regarded to the structural rearrangements that happened upon complex forming, too. Different types of spectrum (1D, 2D homonuclear or hetronuclear experiments) could be used to monitor the changes in the ligand and target molecule resonances in principle, but most conveniently used experiment for the chemical shift mapping is the ^{15}N HSQC measurement of the ^{15}N-labelled protein. The ^{15}N HSQC spectrum clearly show the peaks corresponds to the amide groups and the side-chain NH/NH_2 nitrogen and this provides a fingerprint for the protein. In the titration experiments, a series of ^{15}N HSQC spectra are recorded for the protein sample with increasing the ligand concentrations. The shifts in the position, changes in the linewidth or intensity of the signals indicate change in the chemical environment and this

depends on the Kd. The Kd value can be estimated through non-linear curve fitting of the chemical shift changes versus ligand concentration. ^{15}N HSQC titration can indicate the binding site, and even very weak interactions can be detected and this is one of the advantages of this method.

1.6 Objectives and significance of the study

In an effort to prevent or control development of diseases, which caused by cell death derived from oxidative stress, inflammation, or failure of proliferation signal transduction, including such as AD, prevention of cell death is one of the important and reasonable strategies. Therefore, investigation of molecular mechanisms of cytoprotective activity of HN would beneficial to develop powerful new anti-AD and cytoprotective drugs based on the character of HN and insights of molecular mechanisms of HN-mediated cytoprotection.

This study aims to

- Elucidate the molecular basis of HN-mediated cytoprotective activity in atomic resolution.
- Study the structure-function relationships of Humanin and to elucidate the molecular basis of the anti-amyloid-β fibrillation activity.

2 Experimental

In this chapter I will introduce the different biophysical techniques that have been applied in this thesis, mainly spectroscopic methods.

2.1 Sample preparation

The sufficiently purified (purity: >95%) HN D-Ser14 variant peptides were purchased from Eurofins Genomics (Tokyo, Japan), and were used without further purification. The peptides were dissolved in a 7:3[v/v] H_2O/TFE-d_3 solution and the peptide concentration was adjusted to 2.0 mM as described previously [18,19]. Sufficiently purified (purity: >95%) $A\beta_{40}$ peptide was purchased from Zhejiang Ontores Biotechnologies (Zhejiang, China) and used without further purification.

2.2 Circular dichroism measurements

Far-UV CD spectra (195−250 nm) of 20-μM $A\beta_{40}$ solutions after 4 days of incubation at 25°C with ultrasonication were obtained using a Jasco J-820 spectropolarimeter (Jasco Co., Ltd., Tokyo, Japan) with a quartz cell and a 2-mm path length at 25°C in a 7:3 [v/v] H_2O/TFE solution. Contribution from HN peptides was eliminated subtracting the baseline. CD data were expressed as the mean residue ellipticity.

2.3 Transmission electron microscopy

Sample solution (5 μL) was spotted onto a collodion-coated copper grid (Nisshin EM Co., Tokyo, Japan). After 1 min, the remaining solution was removed with filter paper, and 5 μL of 2% [w/v] ammonium molybdate was spotted onto collodion-coated copper grids. After 1 min, the remaining solution was removed in the same manner as that used above.

Transmission electron microscopy (TEM) (Hitachi H-7650, Tokyo, Japan) images were obtained at 20°C at a voltage of 80 kV and magnification of 10,000.

2.4 NMR spectroscopy

All NMR experiments were performed on Bruker AVANCE III 600 MHz spectrometer equipped with cryogenically cooled probe containing z-axis field-gradient unit at 25 °C of sample temperature. Two-dimensional (2D) ^{1}H-^{1}H TOCSY and ^{1}H-^{1}H NOESY NMR spectra, 2048 data points of F2 dimension and 512 increments with 16 ppm of spectral width in the both dimensions, were recorded with 64 scans in a phase sensitive mode using States-TPPI quadrature detection in the F1 dimension. The mixing time of the ^{1}H-^{1}H NOESY was 160 ms. The DIPSI-2 composite pulse sequence with its mixing period of 80 ms was used for spin locking in the ^{1}H-^{1}H TOCSY measurement. Solvent signals were suppressed by using excitation sculpting pulse scheme [49]. The inter-scan delays of those 2D spectra were 2.0 s. The 2D ^{1}H-^{15}N HSQC spectra, with 1024 data points of F2 (^{1}H) dimension and 94 increments with 16 ppm and 30 ppm of spectral width in the F2 and F1 (^{15}N) dimensions, respectively, were recorded with 360 scans. All of the 2D NMR spectra were processed and analyzed by programs NMRPipe [50] and Sparky (T. D. Goddard and D. G. Kneller, SPARKY 3, University of California, San Francisco), respectively. A pulse-field gradient longitudinal eddy-current delay (PFG-LED) pulse sequence containing bipolar pulse pairs was applied for ^{1}H DOSY experiments [51]. Solvent signals were suppressed by using a presaturation scheme. The diffusion time (Δ) was set to 200 ms. The gradient strength was linearly increased from 1.060 to 51.94 G/cm, and the series of ^{1}H

NMR spectra were obtained with 16 scans and 10 s of inter-scan delay. The ^{1}H DOSY data were processed and analyzed by program TopSpin 3.2 (Bruker).

2.5 Solution structure determination of HN D-Ser

The structure calculation was performed by program CYANA 3.97[52, 53]. A molecular topology description for D-form of serine was prepared by creating mirror images of the cyana residue library using 'library mirror' command of CYANA, and was added to the cyana residue library as an additional entry. The NOE cross peaks in the 2D ^{1}H-^{1}H NOESY spectrum were assigned using the automated NOE assignment algorithm of CYANA. For the NOE assignments, 7 cycles of automated NOE assignment and structure calculation were performed. One hundred structures were calculated and 20 structures with the lowest target function were selected in each cycle. All the NOE assignments were confirmed by visual inspections. A total of 250 upper distance restraints were obtained. With these restraints, 300 structures were calculated and 100 structures with the lowest target function were selected. The selected structures were further refined by program Xplor-NIH 3.21 using a simulated annealing protocol in torsion angle space followed by energy minimization in Cartesian space [54, 55]. The final 20 structures with the lowest energy were selected and verified by program PROCHECK 3.5.4 [56]. An ordered region of the 20 structures was identified by program FitRobot [57]. The secondary structure was assigned by program DSSP 2.1.0[58, 59]. The atomic coordinates and structural restraints (code: waiting for delivery) have been deposited in the Protein Data Bank (http://www.rcsb.org). Electrostatic potential of molecular surface of the HN D-Ser14 variant was calculated using program PyMOL with APBS tools.

2.6 Determination of the amyloid β-binding site of HN D-Ser14

The Aβ binding site of HN was investigated by measuring 2D 1H-15N HSQC spectra of HN (its 15N is natural abundance) with and without $A\beta_{40}$ (molar ratio of HN: $A\beta_{40}$ = 20:1) and by quantifying the signal intensity reduction ratio using Sparky. The error bars of the signal intensity reduction ratio were calculated from the signal-to-noise ratio of individual signals using Sparky. Amino acid residues that showed significant signal intensity reduction were mapped onto a tertiary structure model of HN D-Ser14 using PyMOL.

2.7 Determination of zinc ion binding site on the HN D-Ser14 variant

Zinc ion binding site on the HN D-Ser14 variant was investigated by acquiring natural abundance 2D ^{1}H-^{15}N HSQC spectra of HN D-Ser14 variant and investigating the dose-dependent signal intensity reduction ratio or chemical shift perturbation. The HN D-Ser14 peptide solution as described above was titrated with increasing concentration of $ZnCl_2$ from 2 mM to 128 mM, and natural abundance 2D ^{1}H-^{15}N HSQC spectra of the HN D-Ser14 variant were recorded with each change of zinc ion concentration. Because of the limited solubility of $ZnCl_2$, it was impossible to perform reliable titration experiments using zinc ion concentrations in excess of 128mM. The signal intensity reduction ratio and averaged chemical shift changes (Δδ) of the ^{1}H-^{15}N correlation signals were estimated and compared with the natural abundance 2D ^{1}H-^{15}N HSQC spectra obtained in the absence and presence of 128 mM $ZnCl_2$. The error bars of the signal intensity reduction ratio were calculated from the root sum square of the signal-to-noise ratio of individual signals. The Δδ values were calculated using the equation; $\Delta\delta = ((\Delta\delta_H)^2 + (\Delta\delta_N/5)^2)^{1/2}$, where $\Delta\delta_H$ and $\Delta\delta_N$ represents chemical shift changes (ppm) of amide proton and its ^{15}N nucleus, respectively.

3. Results

3.1. Aβ40 secondary structure analysis by CD spectroscopy

We investigated the secondary structure of $A\beta_{40}$ in the presence and absence of HNs by CD spectroscopy. CD experiments showed that the β-sheet structure of $A\beta_{40}$ was disrupted by mixing HN S14G or HN D-Ser14, relative to the structures in the absence of HN or presence of HN wild-type (Fig 7). In particular, the reduction in the $A\beta_{40}$ β-sheet structure was larger in the presence of HN D-Ser14 than of HN S14G.

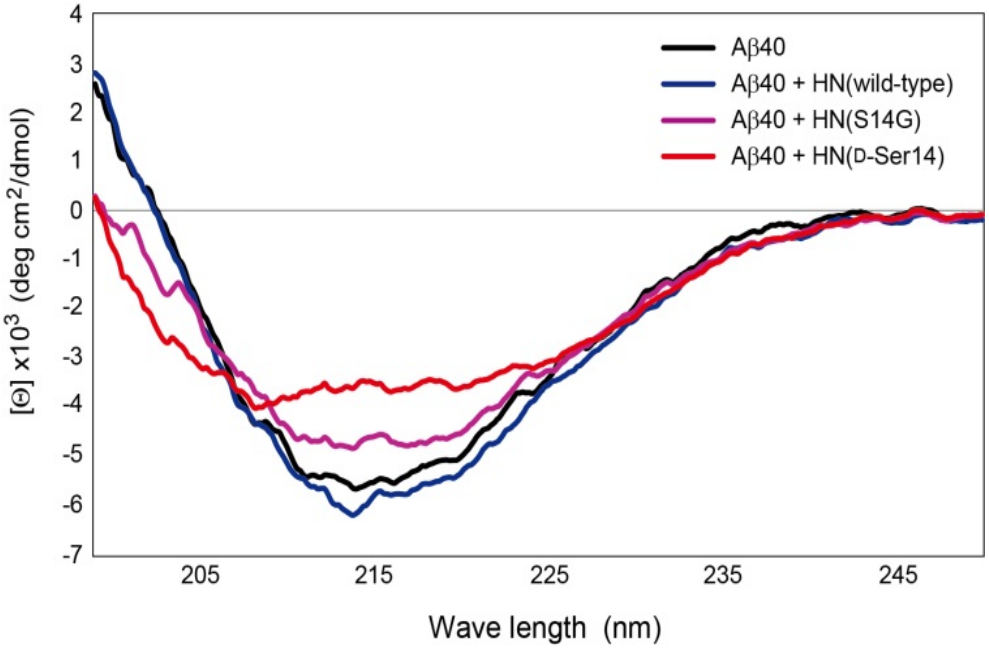

Figure 7. Circular dichroism spectra of $A\beta_{40}$ in the presence ($A\beta_{40}$: HNs = 10:1) or absence of HNs.

3.2 Inhibition of amyloid-β fibrillation by HN wild-type, HN S14G, and HN D-Ser14 observed by TEM

We investigated the fibrillation of $A\beta_{40}$ in the presence or absence of HNs by Transmission electron microscopy (TEM). TEM experiments demonstrated that many fibrils of $A\beta_{40}$ were formed in the absence of HNs (Fig.8). In the presence of HN wild-type or HN S14G, small amounts of Aβ fibrils were formed, but many amorphous-like aggregates were observed. Interestingly, in the presence of HN D-Ser14, Aβ fibrils were not formed, although a small amount of amorphous-like aggregates were observed (Fig.8).

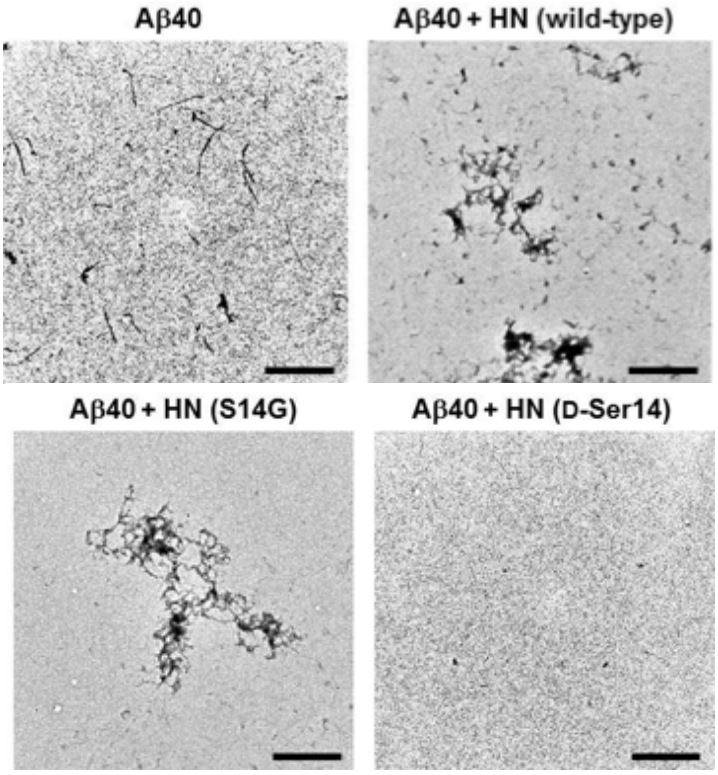

Figure 8. Transmission electron microscopy of $A\beta_{40}$ in the presence ($A\beta_{40}$: HNs = 10:1) or absence of HNs. The image is 2,977 nm by side with scale bar, 600 nm.

3.3 Determination of solution structure of the HN D-Ser14 variant

3.3.1 Resonance assignment

The backbone and side chain ^{1}H signals of HN D-Ser14 variant were assigned using tow-dimensional experiments including, 2D ^{1}H-^{1}H TOCSY and NOESY and . For the 2D experiments, the sample conditions were chosen so as to obtain the best sensitivity and sample stability. After adjusting the suitable conditions for recording the spectra, samples not aggregating and stable over time at the chosen pH and temperature, the 2D spectra were recorded. The backbone and side chain ^{1}H signals of HN D-Ser14 could be completely and unambiguously assigned in a sequential manner through H^{N}-H^{N} NOE signal walking and using the connectivity of inter-residual H^{N}-Hα correlations in the 2D ^{1}H-^{1}H TOCSY and 2D ^{1}H-^{1}H NOESY spectra excluding a few severely degenerated signals (Figure 9). Consequently, inter-proton distance constraints could be collected by analyses of the signal intensities of the 2D ^{1}H-^{1}H NOESY cross-peaks. In addition, natural abundance ^{1}H-^{15}N correlation signals could be completely and unambiguously assigned due to excellent separation of ^{1}H dimension of the amide proton region as shown in (Figure 9).

3.3.2 Structure calculation

The distance restraints that used for the solution structure determination of biomolecule by using NMR are derived primarily from the NOE signals between the protons in the biomolecules at a distance up to 5 Å. NOESY spectrum contains all the information about special proximities of protons and thus encoded the three-dimensional arrangement of atoms, the structure.

All the restraints needed for structure calculation were derived from 2D NOESY experiments. The solution structure of HN D-Ser14 variant was determined based on 250

NOE distance restraints. Residues 5-17 were well converged with the backbone RMSD value of 0.44 Å (Figure 10 A). Other structural statistics are described in Table 2. The residues 6-13 form an α-helix (Figure 10), as revealed by $d\alpha_N$ (i, i+3) NOE connectivity from Phe6 to Leu13 (Figure 10 C). The residues 14-16 adopt a turn conformation as shown by $d\alpha_N$ (i, i+3) NOE connectivity between D-Ser-14 and Asp17 and $d\alpha_N$ (i, i+2) NOE connectivity between Glu15 and Asp17 (Figure 10 C).

Table 2. Experimental restraints and structural statistics for the final 20 structures of HN D-Ser14

Structural restraints	
Total NOEs	250
Short range NOEs (|i-j|≤1)	165
Medium range NOEs (1<|i-j|<5)	65
Long range NOEs (|i-j|≥5)	20
Distance violation	
>0.5 Å	0
Maximum distance violation (Å)	0.28
RMSD to mean coordinates[†]	
Rmsd backbone atoms (Å)	0.44 ± 0.09
Rmsd all atoms (Å)	0.99 ± 0.14
Deviations from idealized covalent geometry	
Rmsd bond lengths (Å)	0.009
Rmsd bond angles (°)	1.5
PROCHECK Ramachandran statistics[††]	
Most favored regions (%)	75.9
Additionally allowed regions (%)	24.1
Generously allowed regions (%)	0.0
Disallowed regions (%)	0.0

[†]calculated for amino acids 5–17

[††]calculated for amino acids 5–13 and 15–17

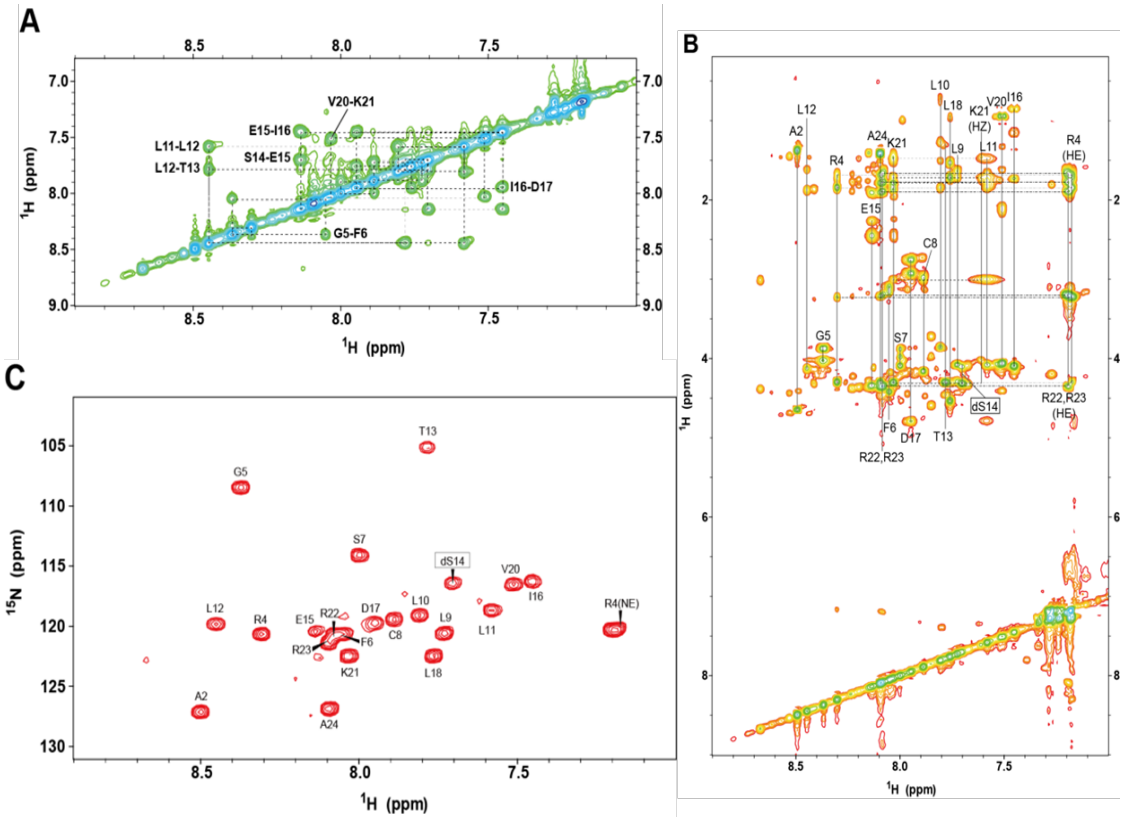

Figure 9. Two-dimensional NMR spectra of the HN D-Ser14. (A) Amide proton region of the 2D ^{1}H-^{1}H NOESY spectrum. Dotted lines denote backbone H^N-H^N NOE connectivity and sequential signal assignments. (B) Fingerprint (aliphatic-amide proton) region of the 2D ^{1}H-^{1}H TOCSY spectrum. Vertical lines denote scalar connectivities of individual amino acid residues. (C) Natural abundance 2D ^{1}H-^{15}N HSQC spectrum. The D-isomerized Ser14 residue is labeled "dS14."

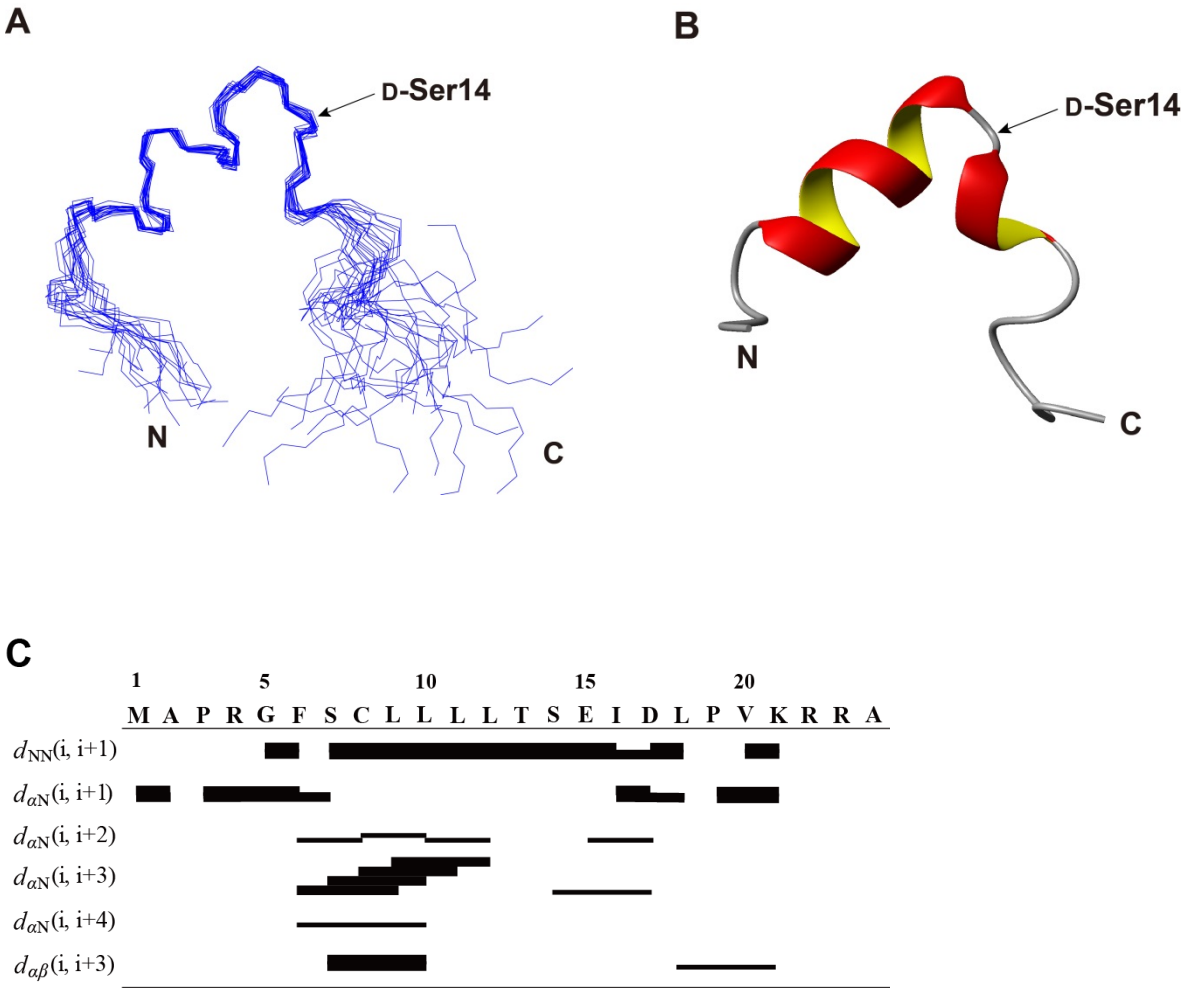

Figure 10. Determination of the solution structure of HN D-Ser14. (A) Backbone superimposition of the 20 energetically lowest NMR structures. (B) Ribbon diagram of the representative structure with the lowest energy. These molecular diagrams were generated using MOLMOL. (C) Schematic summary of sequential NOE connectivities observed in the HN D-Ser14. The thickness of the black bars indicates the intensity of the NOE.

3.4 Oligomeric state of the HN D-Ser14 variant

It was previously proposed that dimerization is important for HN function and interaction with receptors [60]. Therefore, ^{1}H DOSY NMR experiments were performed in order to understand the oligomerization state of HN D-Ser14 variant. Experiments performed at the same condition used for structure determination. From the results of the ^{1}H DOSY NMR experiments we confirmed that the determined solution structure of the HN D-Ser14 was a monomer (Figure 11).

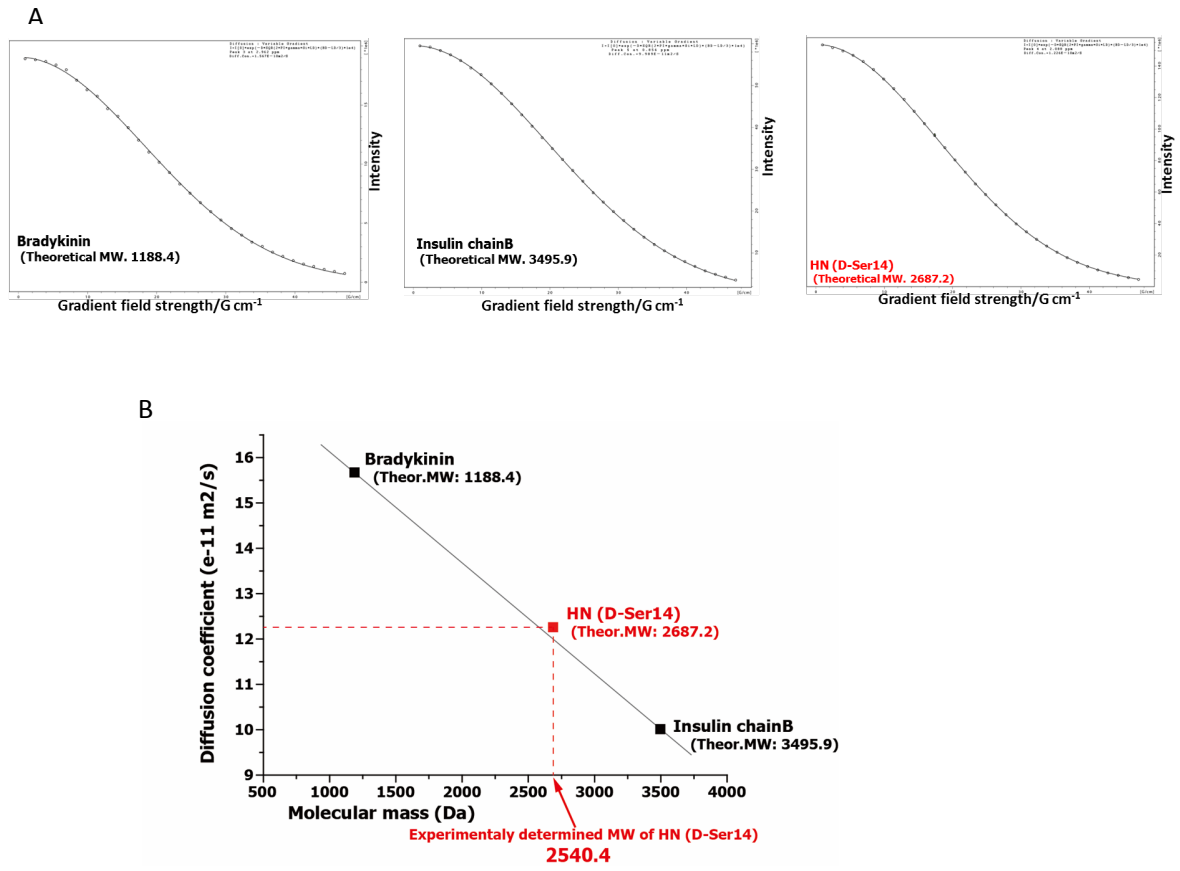

Figure 11. Confirmation of oligomeric state of the HN D-Ser14 under the experimental conditions employed in this study using ^{1}H DOSY NMR. (A) Plot of diffusion-dependent ^{1}H signal intensity attenuation and determination of translational diffusion coefficients of samples by theoretical curve-fitting of the plot. (B) Estimation of the apparent molecular weight of the HN D-Ser14 by comparing the translational diffusion coefficients to those of the 2 other peptides, bradykinin and insulin chain-B (oxidized form), whose translational diffusion coefficients were measured under the same experimental condition with HN D-Ser14 as a molecular weight marker.

3.5 Structural comparison between HN wild-type, HN S14G, and HN D-Ser14

Comparison of the overall structures between HN wild-type, HN S14G, and HN D-Ser14 revealed that all of the three HNs have an α-helix topology (Fig. 12). For HN S14G, however, as previously shown by Benaki et al., the structure between Gly14 and the C-terminus was slightly disordered, relative to that of HN wild-type (Fig. 12) [18]. For HN D-Ser14, on the other hand, the α-helix was sharply bent at the D-Ser14 residue without a disordered α-helix structure of the C-terminal region (Figs. 10 and 12A).

Hydrogen bonding within the backbone between the carbonyl oxygen atom of Leu10 and the amide proton of Thr13 contributed towards formation of the overall straight α-helical structure of HN wild-type (Fig. 12B, left panel). For HN S14G, the plane angle of the peptide bond connecting Thr13 and Ser14 was rotated by approximately 90°, which resulted in the hydrogen bonding partner of the carbonyl oxygen atom of Leu10 being shifted from Thr13 to Gly14 (Fig. 12B, center panel). For HN D-Ser14, the plane angle of the peptide bond connecting Thr13 and D-Ser14 was rotated by approximately 90° in a manner similar to the case of HN S14G (Fig. 12B, right panel). In addition, the plane angle of the peptide bond connecting D-Ser14 and Glu15 was also altered drastically (Fig. 12B, right panel).

The orientations of the backbone amide, side chain methyl, and hydroxyl groups of the Thr13 residue were markedly rearranged, which resulted in the side chain hydroxyl group of the Thr13 being stacked toward the inside of the α-helix and new hydrogen bonds between the side chain hydroxyl group of the Thr13 and backbone amides of D-Ser14 or Glu15 (Fig. 12B, right panel). Finally, five of the packed hydrogen bonds (Leu10-D-Ser14,

Thr13-D-Ser14, Thr13-Glu15, Leu10-Glu15, and Leu10-Ile16) and the hydrophobic contacts between Leu10, Glu15, and Ile16 were newly generated and found to participate in stabilization of the turn structure (Fig. 3B right panel).

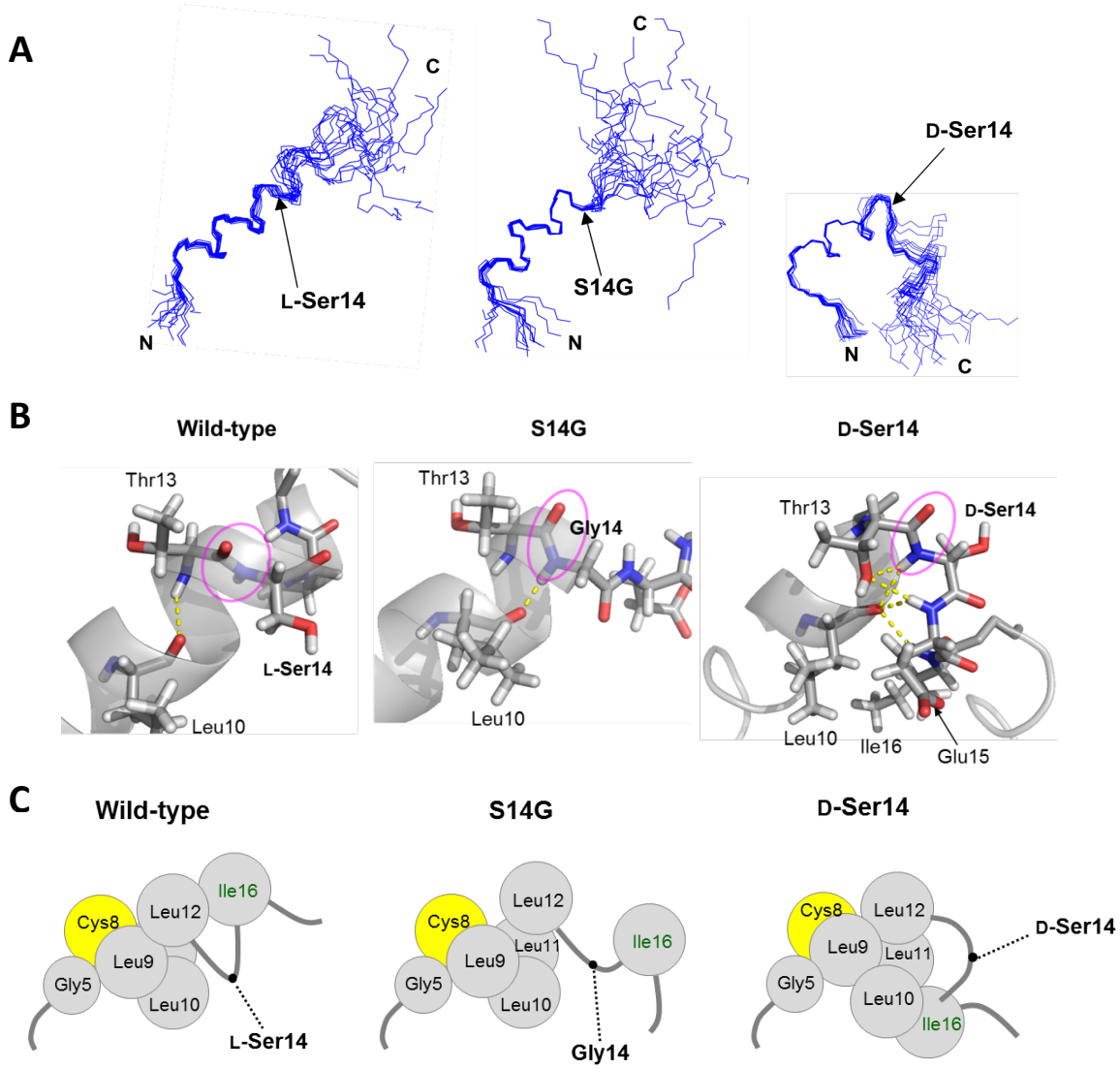

Figure 12. Drastic structural change induced by D-isomerization of the Ser14 residue. (A) Comparison of solution structures of HN wild-type (left panel, PDB code 1Y32), HN S14G (center panel, PDB code 2GD3), and HN D-Ser14 (right panel). (B) Structural detail around the Ser14 residue of HN wild-type (left panel), HN S14G (center panel), and HN D-Ser14 (right panel) showing forces that modulate the structural rearrangement of HN caused by glycine substitution or D-isomerization of the Ser14 residue. The topology of the secondary structure is represented as a transparent ribbon model. Residues Leu10, The13, Ser14, Glu15, and Ile16 are shown as stick models. Amide and oxygen atoms are colored in blue and red, respectively. The yellow dotted lines denote hydrogen bonds. The circles colored in magenta indicate peptide bond moieties linking residues Thr13 and Ser14 (Gly14 in the case of S14G). (C) Schematic views of the structural rearrangement of HN from closed to open form caused by D-isomerization of Ser14. The Cys8 and hydrophobic amino acid residues are shown as spheres on the HN backbone, which is depicted as a transparent ribbon model. Nitrogen and oxygen atoms are colored in blue and red, respectively. The yellow sphere represents the sulfur moiety of the thiol group of Cys8.

3.6 Amyloid β-binding site of HN D-Ser14

In an effort to identify relationships between the variants, we investigated the Aβ-binding sites of HN wild-type, HN S14G, and HN D-Ser14 at atomic resolution by NMR spectroscopy. NMR signals of HN wild-type and HN S14G were not affected by the presence of $A\beta_{40}$ (Figs. 13A and 13B). On the other hand, the intensities of NMR signals of HN D-Ser14 were significantly attenuated by adding $A\beta_{40}$ (Figs. 13A and 13B). These results suggest that the binding affinity for $A\beta_{40}$ is stronger for HN D-Ser14 than for HN wild-type and HN S14G, although accurate determination of the binding affinity was impossible because that of $A\beta_{40}$ was extremely low for HN wild-type and HN S14G, and almost all HN D-Ser14 signals disappeared by adding a small amount of $A\beta_{40}$ in a 10:1 molar ratio of HN: Aβ40.

Amino acid residues that showed significant NMR signal intensity reduction upon binding to Aβ were mapped onto the tertiary structure of HN D-Ser14, as shown in Fig. 13C. The perturbed region formed by Cys8 and Leu9-Leu12 is expected to be the Aβ-binding site of HN D-Ser14. This interpretation is consistent with a previous study using limited proteolysis and mass spectroscopic analyses of an HN–Aβ mixture that indicated that the Aβ-binding site of HN contained Leu9-Leu12 [61]. The ^{1}H-^{15}N correlation signals of residues Gly5, Cys8, Leu9, Leu10, and Leu12 were markedly line-broadened upon addition of zinc ions (Fig. 15), which indicated that Cys8 and Leu9-Leu12 are involved in both Aβ and zinc ion binding. Zinc ions have been found to be the most abundant trace metal in brain tissue, and HN bound to zinc ions [44]. These ions have been shown to accelerate aggregation or fibrillation of Aβ [42, 43], and such accelerations were suppressed by HN [44]. Our data showed that HNs were involved in Aβ and zinc ion binding, which may explain why HN suppresses the zinc-promoted aggregation or fibrillation of Aβ.

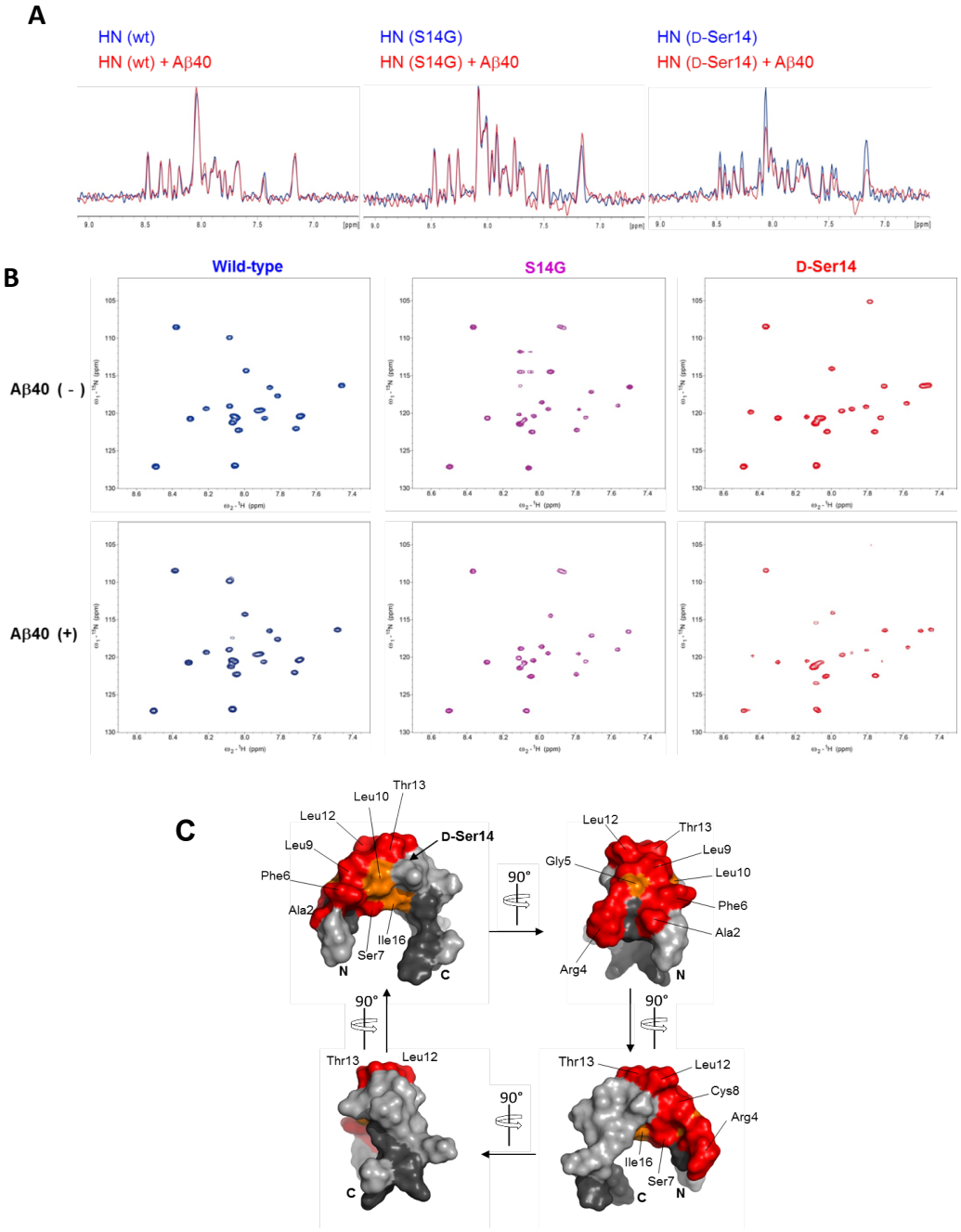

Fig.13. Difference in Aβ recognition mode between the HN variants and identification of the Aβ binding site on HN D-Ser14. (A) Overlay of 1D ^{15}N-edited ^{1}H NMR spectra of HN wild-type, HN S14G, and HN D-Ser14 (left, center, and right panels, respectively) in the absence or presence of $A\beta_{40}$ (colored in blue and red, respectively). (B) 2D ^{1}H-^{15}N HSQC spectra of the HN wild-type, HN S14G, and HN D-Ser14 (colored in blue, magenta, and red, respectively) in the absence or presence of $A\beta_{40}$. Plots of signal intensity ratios of whole amino acid residues are shown in Supplementary Fig. S4. (C) Mapping of residues that showed significant intensity attenuation of ^{1}H-^{15}N correlation signals on the surface representations of the HN D-Ser14 structure. Red and orange surfaces indicate residues displaying signal intensity ratios of <0.6 and 0.6–0.7, respectively. Dark gray surfaces indicate no data region (Met1, Pro3, and Pro20).

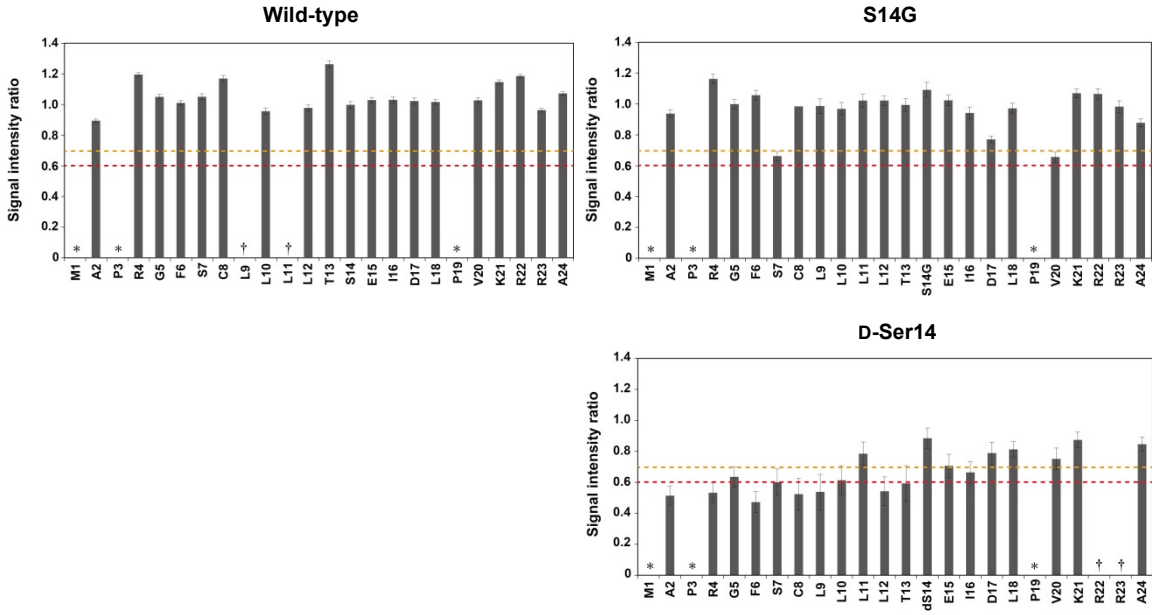

Fig. 14. Signal intensity ratio of 2D ^{1}H-^{15}N HSQC spectra of individual amino acid residues induced by addition of $A\beta_{40}$. Dashed lines indicate threshold of 0.60 (red) and 0.70 (orange). The obelisks indicate that accurate estimation of signal intensity was impossible because of degeneracy of signals (i.e., L9 and L11 of wild-type, R22 and R23 of HN D-Ser14). The asterisks indicate no ^{1}H-^{15}N correlation signals (Met1, Pro3, and Pro20). The molar ratios of HNs and Aβ40 were 20:1 in those experiments. Error bars were calculated on the basis of the signal-to-noise ratio of the individual signal.

3.7 Identification of zinc ion binding site on the HN D-Ser14 variant

Many report have shown that zinc ion plays a harmful role in progression of AD promoting aggregation of Aβ [42]. Structural characterization of the ligand binding site and identification of the amino acid involved in the direct recognition of zinc ion on the HN D-Ser14 had been carried out.

The amide resonances are suitable probes for studying macromolecular interactions because it is very sensitive; the chemical shift is sensitive to both direct interactions with a binding partner and to the induced conformational changes in the macromolecule, Taking advantage of the complete assignments of natural abundance ^{1}H-^{15}N NMR signals of the HN D-Ser14, we performed a series of HSQC based NMR titration experiments, and amino acid residues whose signal intensity and chemical shift value of their ^{1}H-^{15}N signals were severely altered upon binding to zinc ion were mapped onto the HN D-Ser14 tertiary structure model (Figure 15). As a result, ^{1}H-^{15}N correlation signals of Cys8, Leu9, Leu10 and Leu12 residues were specifically disappeared, and the signal of Gly5 was remarkably broadened upon recognition of zinc ion (Figure 15B and 4D). For the Significant signal broadening that observed at Cys8, Leu9, Leu10 and Leu12 residues, it is assumed that the specific and extreme signal line-broadening of these residues were caused due to chemical exchange between apo- and complex forms in an intermediate rate with respect to the NMR time scale. It indicates that those four residues are involved in direct binding to zinc ion. Those results would be supported by previous study by performing mutagenesis assay that the Cys8 of the parent HN constitutes its zinc ion binding site [44].

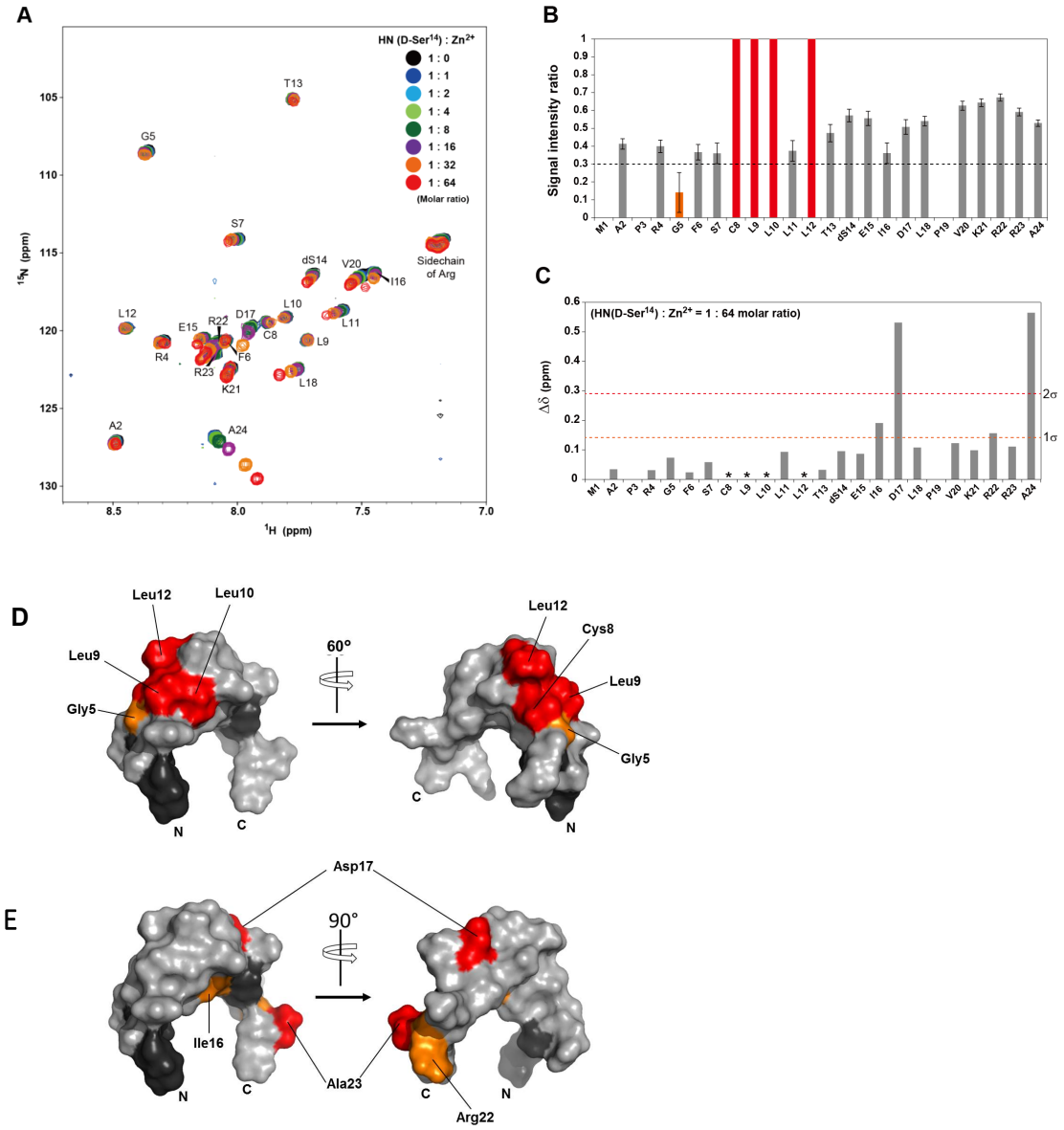

Figure 15. Identification of the zinc ion binding site on HN D-Ser14. (A) Superimposed 2D ^{1}H-^{15}N HSQC spectra of HN D-Ser14 in the absence or presence of various concentrations of zinc ion, as shown in the inset. (B) Signal intensity ratio of 2D ^{1}H-^{15}N HSQC spectra of individual amino acid residues induced by addition of zinc ion. Dashed line indicates a threshold of 0.30. Red bars indicate completely broadened out ^{1}H-^{15}N correlation signals caused by addition of 128-mM zinc ions. (C) Normalized chemical shift changes (Δδ) of 2D ^{1}H-^{15}N HSQC spectra of individual amino acid residues induced by addition of zinc ions. Orange and red dashed lines indicate thresholds of 1σ and 2σ, respectively; σ is the standard deviation of the chemical shift change. (D) Mapping of residues with significantly broadened ^{1}H-^{15}N correlation signals by titration of zinc ions on the CPK (upper panel) and surface (lower panel) representations of the HN D-Ser14 structure. Red and orange surfaces indicate residues with severely broadened signals and reduced signal intensities, respectively. (E) Mapping of residues that showed significant chemical shift changes by addition of zinc ions. The asterisks indicate completely broadened ^{1}H-^{15}N correlation signals caused by addition of 128-mM zinc ions

4. Discussion

4.1 Structural modulation of Aβ by HN D-Ser14

The CD spectra of Aβ with and without HNs indicated that the secondary structure of Aβ was clearly altered toward a conformation that was inadequate for nucleation/seeding of Aβ fibrillation by interaction with HNs; the order of potency was HN D-Ser14 > HN S14G > HN wild-type (Fig.7). In addition, TEM images of Aβ fibrillation profiles with and without HNs showed that HNs inhibited Aβ fibrillation, and the order of potency was HN D-Ser14 > HN S14G > HN wild-type (Fig. 8).

4.2 Structural impact of D-isomerization of HN

As shown on figure 12, the optical isomerization of Ser14 from the L to D form disrupted the extended α-helix topology of HN at the D-Ser14 residue and introduced a turn conformation within the D-Ser14 and Ile16 region (figure 12, 16). Under the same experimental conditions, it has been reported that HN S14G also forms an α-helical structure spanning Phe6 to Thr13, and substitution of Ser14 to Gly14 breaks the helix and leads to structural disorder of the downstream region from Gly14 [19].

The drastic structural change facilitated by D-isomerization of Ser14 reorganized hydrophobic contact between Leu10 and Ile16 (Fig. 12 and 16). For HN wild-type, side chains of Leu12 and Ile16 form hydrophobic contact, which helps stabilize straight helix formation (Fig. 16A). On the other hand, for HN S14G and HN D-Ser14, we found that the Leu12-Ile16 hydrophobic contact was disrupted by Ser14Gly substitution and that the

hydrophobic interaction partner of Ile16 was shifted from Leu12 to Leu10 following backbone bending caused by D-Ser14 (Figs. 16B, C).

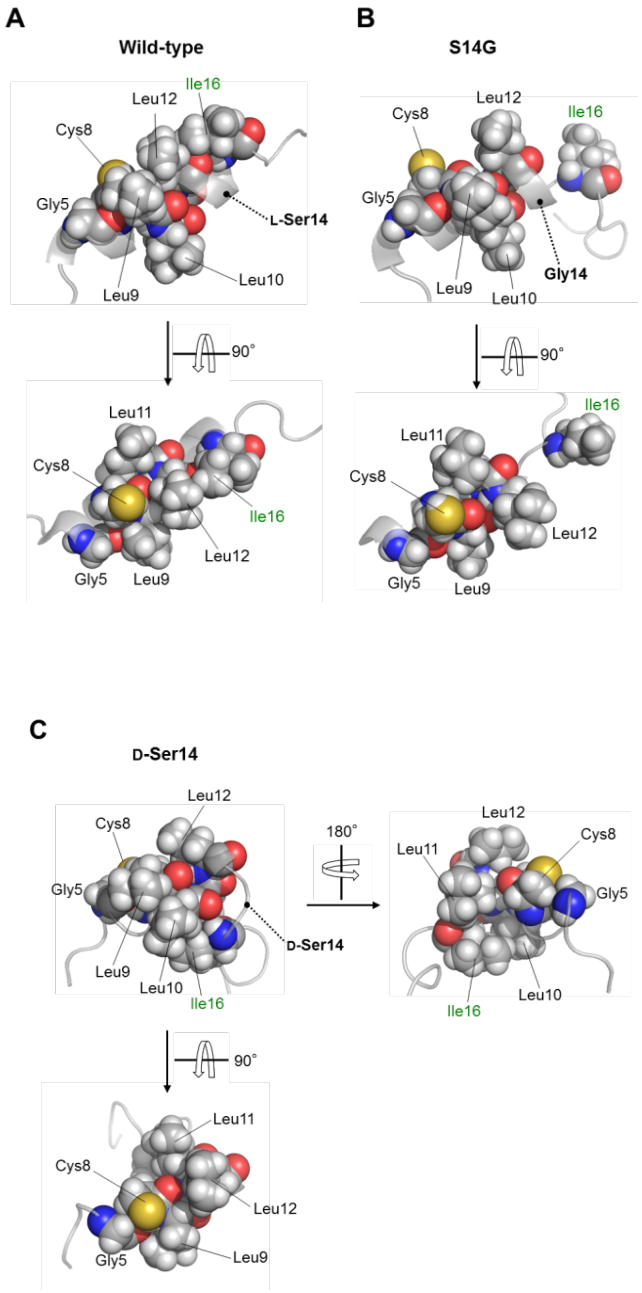

Fig16. Structural rearrangement of HN from closed to open form caused by D-isomerization of Ser14. (A) HN wild-type, (B) HN S14G, and (C) HN D-Ser14. The Cys8 and hydrophobic amino acid residues are shown as spheres on the HN backbone, which is depicted as a transparent ribbon model. Nitrogen and oxygen atoms are colored in blue and red, respectively. The yellow sphere represents the sulfur moiety of the thiol group of Cys8.

4.3 Aβ recognition by HNs

As described above, among the 3 HN variants investigated, HN D-Ser14 showed the strongest inhibitory activity against the progress of aggregation/fibrillation of Aβ (Figs. 7, 8), and has a characteristic structure (Figs. 10, 12). Because the reported tertiary structures of HN wild-type and HN S14G were determined in an alcohol/water mixture [9, 10], a HN binding partner should be analyzed in such a mixture for use in a structure–function correlation study. Physicochemical and structural studies of Aβ in alcohol/water mixtures have been widely conducted [12]. From the result of Aβ interaction with HNs (fig13, 14), region formed by Cys8 and Leu9-Leu12 is expected to be the Aβ-binding site of HN D-Ser14. This interpretation is consistent with a previous study using limited proteolysis and mass spectroscopic analyses of an HN–Aβ mixture that indicated that the Aβ-binding site of HN contained Leu9-Leu12 [61]. The ^{1}H-^{15}N correlation signals of residues Gly5, Cys8, Leu9, Leu10, and Leu12 were markedly line-broadened upon addition of zinc ions (Fig. 15), which indicated that Cys8 and Leu9-Leu12 are involved in both Aβ and zinc ion binding.

As shown in figure 13, the signal broadening induced by Aβ is on the order of HN D-Ser14 >> HN S14G > HN wild-type, which is basically consistent with previous reports stating that HN S14G and HN D-Ser14 exhibited stronger cytoprotective activity than that of HN wild-type [4,24]. Furthermore, the magnitude of the conformational differences among HN wild-type, HN S14G, and HN D-Ser14 appeared to be related to differences in cytoprotective activity and binding affinity for Aβ (Figs. 7, 8, 12, 13).

4.4 Zinc ion binding to HN D-Ser14

In many cases, it is well known that nitrogen atoms of indol group of histidine, oxygen atoms of hydroxyl group of glutamate and aspartate, and thiol group of cysteine residues play a role as donor atoms of zinc ion [62]. As described above, zinc ion is abundantly exists in amyloid plaques in brain of AD patients, and it is well known that Aβ-zinc ion interaction significantly influence pathogenesis of AD [42]. Therefore it is assumed that interaction between HN and zinc ion affects physicochemical properties of Aβ and it is one of the mechanisms of neuroprotective activity of HN [44]. In many cases, thiol group of cysteine residue plays role in redox center of polypeptides, and its oxidation or reduction states are switched by binding of zinc ion although zinc ion itself is redox-silent. Therefore, binding zinc ion with thiol group of cysteine regulates redox activity of the cysteine, and thereby it modulates polypeptide's structural conformation and enzymatic activity in response to oxidative stress and changing redox circumstances [63]. It is widely known that oxidative stress is associated with many kind of cell death [64]. Therefore, it is considered that binding of zinc ion to the Cys8 residue of HN is important to exert neuroprotective and globally cytoprotective actions against AD- and oxidative stress-related cell death, respectively. At present, transition metal ion, which is reported to participate in direct interaction and functional cooperation with HN, is zinc only [44]. On the other hand, Aβ binds to copper and iron ions in addition to zinc [42]. As a general mechanism, the majority of reactive oxygen species (ROS) are generated from resulting unmanaged inappropriate redox chemical reaction between molecular oxygen and redox-active metal ions, such as copper and iron [65]. Aβ surely reduces those metal ions and it results generation of ROS in brain, which is the most high oxidative organs, and thereby it

mediates cytotoxicity. As for the zinc ion, on the other hand, binding redox-silent zinc ion to Aβ as displacing copper ions from Aβ attenuates cytotoxicity of Aβ by suppressing Aβ-mediated ROS production [66]. As a result of our study, it was demonstrated that affinity between HN D-Ser14 variant and zinc ion was significantly lower than the case of parent HN. It suggests that HN D-Ser14 variant does not interfere Aβ-zinc ion interaction and does not influence local zinc ion concentration compared to the case of parent HN. Its character may contribute to aggressive or enhancement effects for Aβ-zinc ion interaction at the functional cross-talk between Aβ, HN, and zinc ion, and thereby it is possible that the character is one of the fundamental mechanisms of potent cytoprotective activity of HN D-Ser14 variant. Incidentally, it was considered that multimeriation or aggregation of HN D-Ser14 were not occurred along with titration of zinc ion since linearly zinc ion concentration-dependent general line broadening of NMR signals were not observed. Considering structural characters of the elucidated HN D-Ser14 variant, the zinc ion binding site is close to the five hydrogen bonds and hydrophobic contact sites of the HN D-Ser14 variants (Figure 12 and 15). Especially, Leu10 participates in forming all of the three sites, zinc ion binding site, five hydrogen bonds, and hydrophobic contact site of the HN D-Ser14 variant. Therefore, it is possible that binding zinc ion to HN induces conformational changes at around the Leu10 containing the five hydrogen bonds and hydrophobic contact site, and thereby it regulates interaction between HN D-Ser14 and its functional partners. The contrary is also possible that conformational change is induced at the zinc ion binding site of the HN upon interaction with functional partner, it results that zinc ion binding mode of the HN is modulated in the direction of more favorable conformation for zinc ion recognition. In addition to the prominent signal broadening,

significant chemical shift changes were also observed at Ile16, Asp17, Arg22, and Ala24 in C-terminal region upon interaction to zinc ion (Figure 15). Since hydroxyl group of aspartate also has a potential to coordinate zinc ion [62], it is possible that the Asp17 also participate in binding to zinc ion. However, from the difference of the alteration profiles of NMR signals between the Cys8 and Asp17 upon binding to zinc ion, NMR signals of the former and latter were severely broadened and prominently moved its chemical shift, respectively, it is considered that exchange rate between the Asp17 and zinc ion is more fast rather than the Cys8-zinc ion interaction. Therefore, it is possible that the Asp17 is second binding site of zinc ion. This is first report of clearly revealing the Asp17 plays role in interaction between HN and zinc ion. On the other hands, it is also assumed that significant chemical shift changing of the around of the Asp17, which are Ile16, Arg22, and Ala24, were caused by altering their chemical environment or structural rearrangement in like an induced-fit manner according to Asp17-zinc ion interaction. NMR analyses of dynamics of structural fluctuation such as relaxation analyses of backbone ^{15}N nucleus magnetization of target polypeptides provide important insights about structure-function relationship. In this study, however, performing such experiments were extremely difficult since preparation of recombinant polypeptides containing D-amino acid by using general protein expression methods is technically almost impossible, and chemical synthesis of sufficient amount of isotopically-enriched polypeptide was economically impossible. However, we could only estimate an approximate order of magnitude of affinity for zinc ion due to their weak binding. In previously, it has been reported that zinc ions bind to HN with apparent affinity in the low μM range of dissociation constants [44].

4.5 Electrostatic potential of HNs surface

Electrostatic potential map of the molecular surface of HNs indicates that the N- and C-terminal regions of HNs are positively charged, and the core region between the terminals has negatively charged or neutral surface electrostatic potentials (Fig. 17). In the case of the HN D-Ser14, the spatial distance between the N- and C-terminal regions, both of which have electrostatically positive surface potentials in common with those of the HN wild-type and HN S14G, is shorter as a result of the drastic conformational change, thereby resulting in clear polarization of the whole globular molecule of the HN D-Ser14 (Fig. 17C).

These results indicate that the area of electrostatically neutral or hydrophobic surface on the Aβ-binding site of the HN D-Ser14 variant was increased from those of the HN wild-type and HN S14G (denoted as green circles in Fig. 17). The findings are supported by previous reports stating that hydrophobic binding mainly contributes to the HN–Aβ interaction [61]. However, by comparing the solvent accessibility of each amino acid residue between HNs, there was no increase in solvent accessibility of the hydrophobic patch of the Aβ-binding site of HN D-Ser14 (Fig. 17D), which means that the electrostatic charge profile of the hydrophobic patch on the Aβ-binding site of HN was rearranged in addition to reorganization of the hydrophobic packing network inside HN caused by the drastic conformational change upon D-isomerization of the Ser14 residue.

Interestingly, solvent accessibility of Leu10, which is the central core residue of the hydrophobic patch on the Aβ-binding site of HN, became smaller in the order of HN D-Ser14, HN S14G, NH wild-type (Fig. 17D). These results are consistent with differences in the Aβ-binding avidity and Aβ fibrillation inhibition potency between the HN variants. Overall, the results indicate that the Leu10 residue contributes significantly to allowing

conformational and physicochemical characteristic changes in the hydrophobic patch on the Aβ-binding site of the HN to give a more adequate form for binding to Aβ, even if the Leu10 residue does not participate in direct recognition of Aβ (Fig. 13).

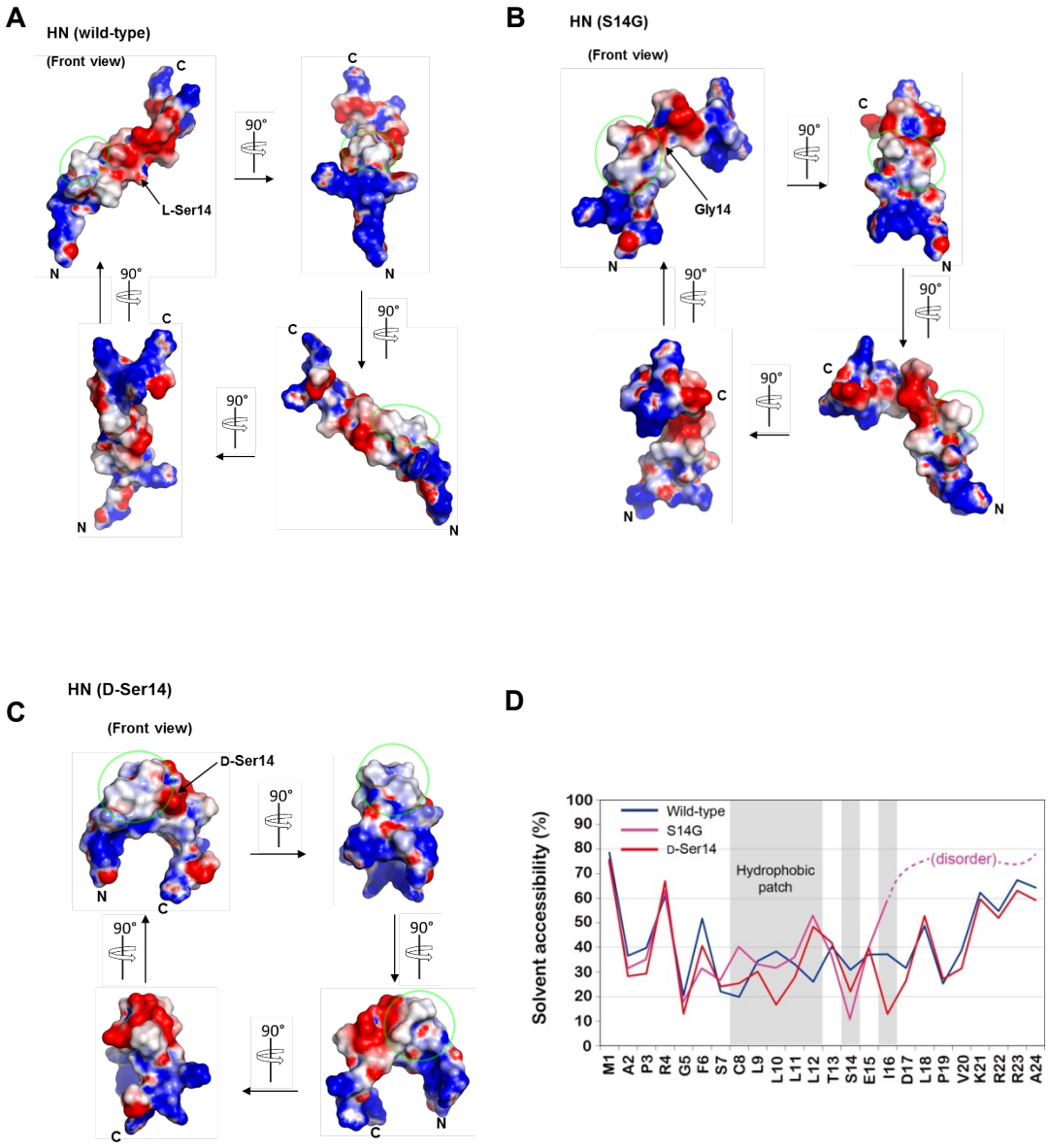

Figure. 17. Electrostatic potential of the molecular surfaces of HN wild-type (A), HN S14G (B), and HN D-Ser14 (C). Positively and negatively charged areas are colored in blue and red, respectively. The surface electrostatic potential was calculated using PyMOL with APBS tools (±4 *kT* scale). Green circles indicate hydrophobic patches in the Aβ-binding site. (D) Comparison of solvent accessibility among HN wild-type, HN S14G, and HN D-Ser14. Gray-colored background indicates Leu9-Leu12 (forming hydrophobic patch), Ser14, and Ile16 residues.

5 Concluding remarks

Elucidating the molecular mechanism of the cytoprotective activity of Humanin peptide have been a main goal of this thesis. In addition, the differences in structure and function between the HN wild-type, HN S14G, and HN D-Ser14 ware carefully compared. Efforts have been directed to understand the correlation between the structure and function of the HNs. This chapter will state the main conclusions from this thesis aiming to put them into perspective.

In this thesis, an approach using different biophysical techniques has provided deep insights into the cytoprotective action of HN. We used Aβ as a binding partner of Humanin.

We acquired circular dichroism (CD) spectra and performed electron microscopy of Aβ in the presence or absence of the HN variants to investigate how Aβ aggregation and/or fibrillation are influenced by interacting with HN wild-type, HN S14G, or HN D-Ser14. The study revealed that Humanin can alter the secondary structure of Aβ40 and therefore inhibits the Aβ fibrillation and HN D-Ser14 have a strong inhibitory activity against the progress of fibrillation.

A high-resolution tertiary structure of HN D-Ser14 was determined under the same solution condition as that used for the HN wild-type and HN S14G (alcohol/water mixture) and our study revealed that HN D-Ser14 forms monomeric helical structure in lipophilic environment, and it was elucidated that the potent enhancement of the cytoprotective activity is based on the drastic conformational change to the HN at the position of the Ser14, which was caused by site-specifically D-isomerization of the Ser14 residues.

The binding modes between Aβ and the HNs were elucidated at atomic resolution by performing solution NMR experiments and the HN D-Ser14 possess a strong binding affinity for $A\beta_{40}$. It is considered that interaction between Aβ, HN, and zinc ion have an important consequence for pathogenesis of AD. For the first report, furthermore, zinc ion binding site on the HN D-Ser14 could be determined. The results of this study would provide valuable insights in an effort to develop efficacious new drugs against age-related incurable diseases.

References

1. Nunnaril, J. & Suomalainen, A., Mitochondria: in sickness and in health, *Cell* **148**, 1145–1159 (2012).

2. Cobb, L. J., Lee, C., Xiao, J., Yen, K., Wong, R. G., Nakamora, H. K., Mehta, H. H., Gao, Q., Ashur, C., Huffman, D. M., Wan, J., Muzumdar, R., Brazilai, N & Cohen, P. Naturally occurring mitochondrial-derived peptides are age-dependent regulators of apoptosis, insulin sensitivity, and inflammatory markers. *Aging* **8,** 796-809 (2016).

3. Lee, C., Yen, K., & Cohen, P. Humanin: a harbinger of mitochondrial-derived peptides?. *Trends Endocrinol Metab* **24**, 222-228 (2013).

4. Hashimoto, Y., Niikura, T., Tajima, H., Yasukawa, T., Sudo, H., Ito, Y., Kita, Y., Kawasumi, M., Kouyama, K., Doyu, M., Sobue, G., Koide, T., Tsuji, S., Lang, J., Kurokawa, K., & Nishimoto, I. A rescue factor abolishing neuronal cell death by a wide spectrum of familial Alzheimer's disease genes and Abeta. *Proc Natl Acad Sci U S A* **98**, 6336-6341(2001).

5. Guo, B., Zhai, D., Cabezas, E., Welsh, K., Nouraini, S., Satterthwait, A. C., & Reed, J. C. Humanin peptide suppresses apoptosis by interfering with Bax activation. *Nature* **423**, 456-461(2003).

6. Ikonen, M., Liu, B., Hashimoto, Y., Ma, L., Lee, K. W., Niikura, T., Nishimoto, I., & Cohen, P. Interaction between the Alzheimer's survival peptide humanin and insulin-like growth factor-binding protein 3 regulates cell survival and apoptosis. *Proc Natl Acad Sci U S A* **100**, 13042-13047 (2003).

7. Lee, C., Zeng, J., Drew, B. G., Sallam, T., Martin-Montalvo, A., Wan, J., Kim, S. J., Mehta, H., Hevener, A. L., de Cabo, R., & Cohen, P. The mitochondrial-derived peptide MOTS-c promotes metabolic homeostasis and reduces obesity and insulin resistance. *Cell Metab* **21**, 443-454 (2015).

8. Nishimoto, I., Matsuoka, M., & Niikura, T. Unravelling the role of Humanin. *Trends Mol Med* **10**,102–105 (2004).

9. Zhao, S. T., Zhao, L., & Li, J. H. Neuroprotective Peptide humanin inhibits inflammatory response in astrocytes induced by lipopolysaccharide. *Neurochem Res* **38**, 581-588 (2013).

10. Yen, K., Lee, C., Mehta, H., & Cohen, P. The emerging role of the mitochondrial-derived peptide humanin in stress resistance. *J Mol Endocrinol* **50**, R11-R19 (2013).

11. Gong, Z., Tas, E., & Muzumdar, R. Humanin and age-related disesese: a new link?. *Endocrinology* **5**: 210 (2014).

12. Zhai, D., Luciano, F., Zhu, X., Guo, B., Satterthwait, A. C., & Reed, J. C. Humanin binds and nullifies Bid activity by blocking its activation of Bax and Bak. *J Biol Chem* **280**, 15815-15824 (2005).

13. Hashimoto, Y., Kurita, M., Aiso, S., Nishimoto, I., & Matsuoka, M. Humanin inhibits neuronal cell death by interacting with a cytokine receptor complex or complexes involving CNTF receptor alpha/WSX-1/gp130. *Mol Biol Cell* **20**, 2864-2873 (2009).

14. Matsuoka, M., & Hashimoto, Y. Humanin and the receptors for humanin. *Mol Neurobiol* **41**, 22-28 (2010).

15. Ying, G., Iribarren, P., Zhou, Y., Gong, W., Zhang, N., Yu, Z. X., Le, Y., Cui, Y., & Wang, J. M. Humanin, a newly identified neuroprotective factor, uses the G protein-coupled formylpeptide receptor-like-1 as a functional receptor. *J Immunol* **172**, 7078-7085 (2004).

16. Niikura, T., Hashimoto, Y., Tajima, H., Ishizaka, M., Yamagishi, Y., Kawasumi, M., Nawa, M., Terashita, K., Aiso, S., & Nishimoto, I. A tripartite motif protein TRIM11 binds and destabilizes Humanin, a neuroprotective peptide against Alzheimer's disease-relevant insults. *Eur J Neurosci* **17**, 1150–1158 (2003).

17. Rossini, L., Hashimoto, Y., Suzuki, H., Kurita, M., Gianfriddo, M., Scali, C., Roncarati, R., Franceschini, D., Pollio, G., Trabalzini, L., Terstappen, G.C., Matsuoka, M., & Caricasole, A. VSTM2L is a novel secreted antagonist of the neuroprotective peptide Humanin. *FASEB J* **25**, 1983–2000 (2011).

18. Benaki, D., Zikos, C., Evangelou, A., Livaniou, E., Vlassi, M., Mikros, E., & Pelecanou, M. Solution structure of humanin, a peptide against Alzheimer's disease-related neurotoxicity. *Biochem Biophys Res Commun* **329**, 152-160 (2005).

19. Benaki, D., Zikos, C., Evangelou, A., Livaniou, E., Vlassi, M., Mikros, E., & Pelecanou, M. Solution structure of Ser14Gly-humanin, a potent rescue factor against neuronal cell death in Alzheimer's disease. *Biochem Biophys Res Commun* **349**, 634-642 (2006).

20. Mehrnejad, F., & Chaparzadeh, N. Structural and dynamical studies of Humanin in water and TFE/water mixture: a molecular dynamics simulation. *J Biomol Struct Dyn* **26**, 255-262(2008).

21. Niikura, T., Chiba, T., Aiso, S., Matsuoka, M., & Nishimoto, I. Humanin: after the discovery. *Mol Neurobiol* **30**, 327-340 (2004).

22. Yamagishi, Y., Hashimoto, Y., Niikura, T., & Nishimoto, I. Identification of essential amino acids in Humanin, a neuroprotective factor against Alzheimer's disease-relevant insults, *Peptides* **24**, 585-595 (2003).

23. Arakawa, T., Niikura, T., Tajima, H., & Kita, Y. The secondary structure analysis of a potent Ser14Gly analog of antiAlzheimer peptide, Humanin, by circular dichroism, *J Pept Sci* **12**, 639-642 (2006).

24. Terashita, K., Hashimoto, Y., Niikura, T., Tajima, H., Yamagishi, Y., Ishizaka, M., Kawasumi, M., Chiba, T., Kanekura, K., Yamada, M., Nawa, M., Kita, Y., Aiso, S., & Nishimoto, I. Two serine residues distinctly regulate the rescue function of Humanin, an inhibiting factor of Alzheimer's disease-related neurotoxicity: functional potentiation by isomerization and dimerization, *J Neurochem* **85**, 1521-1538 (2003).

25. Heck, S., Faraci, W., Kelbaugh, P., Saccomano, N., Thadeio, P., & Volkmann, R.

Posttranslational amino acid epimerization: Enzyme-catalyzed isomerization of amino acid residues in peptide chains. *Proc Natl Acad Sci U S A* **93**, 4036-4039 (1996).

26. ALZHEIMER, A. Über eine eigenartige Erkrankung der Hirnrinde. Allg. Z. Psychiat. Psych.-Gerichtl. *Med*. **64**,146–148 (1907).

27. Haass, C. & Selkoe, D. J. Soluble protein oligomers in neurodegeneration: lessons from the Alzheimer's amyloid beta-peptide. *Nat Rev Mol Cell Biol* **8**, 101–112 (2007).

28. Hardy, J., & Selkoe, D. J. The amyloid hypothesis of Alzheimer's disease: progress and problems on the road to therapeutics. *Science* **297,** 353–356 (2002).

29. Cohen, S.I.A., Linse, S., Luheshi, L.M., Hellstrand, E., White, D.A., Rajah, L., Otzen, D.E., Vendruscolo, M., Dobson, C.M., & Knowles, T.P.G. Proliferation of amyloid-β42 aggregates occurs through a secondary nucleation mechanism. *Proc Natl Acad Sci USA* **110**, 9758-9763 (2013).

30. Glenner, G. G., & Wong, C. W. Alzheimer's disease: initial report of the purification and characterization of a novel cerebrovascular amyloid protein. *Biochem Biophys Res Commun* **120**, 885–890 (1984).

31. Prince, M., Bryce, R., Albanese, E., Wimo, A., Ribeiro, W., & Ferri, C. P. The global prevalence of dementia: A systematic review and metaanalysis. *Alzheimer's & Dementia* **9**, 63–75 (2013).

32. Rajasekhar, K., Chakrabartia, M., & Govindaraju, T. Function and toxicity of amyloid beta and recent therapeutic interventions targeting amyloid beta in Alzheimer's disease. *Chem. Comm* **51**, 13434–13450 (2015).

33. Savelieff, M. G., Lee, S., Liu, Y., & Lim, M. H. Untangling amyloid-β, Tau, and metals in Alzheimer's disease. *ACS Chem. Biol*. **8**, 856–865 (2013).

34. De Toma, A. S., Salamekh, S., Ramamoorthy, A., & Lim, M. H. Misfolded proteins in Alzheimer's disease and type II diabetes. *Chem.Soc. Rev.* **41**, 608–621 (2012).

35. Kotler, S. A., Brender, J. R., Vivekanandan, S. 1., Suzuki, Y., Yamamoto, K., Monette, M., Krishnamoorthy, J., Walsh, P., Cauble, M., Holl, M. M., Marsh, E. N., & Ramamoorthy, A. High-resolution NMR characterization of low abundance oligomers of amyloid-β without purification. *Sci. Rep*. **5**, 11811 (2015).

36. Kotler, S. A., Walsh, P., Brender, J. R., & Ramamoorthy, A. Differences between amyloid-β aggregation in solution and on the membrane: insights into elucidation of the mechanistic details of Alzheimer's disease. *Chem. Soc. Rev*. **43**, 6692–6700 (2014).

37. Adlard, P. A., & Bush, A. I. Metals and Alzheimer's disease. *J Alzheimers Dis* **10,**145–163 (2006).

38. Lovell, M. A., Robertson, J. D., Teesdale, W. J., Campbell, J. L., & Markesbery, W. R. Copper, iron and zinc in Alzheimer's disease senile plaques. J Neurol Sci 158, 47–52 (1998).

39. Faller, P. Copper and zinc binding to amyloid-beta: coordination, dynamics, aggregation, reactivity and metal-ion transfer. *ChemBioChem* **10** 2837–2845 (2009).

40. Faller, P. & Hureau, C. A bioinorganic view of Alzheimer's disease: when misplaced metal ions (re)direct the electrons to the wrong target. *Chemistry* **18**, 15910–15920 (2012).

41. Miller, L. M., Wang, Q., Telivala, T. P., Smith, R. J., Lanzirotti, A., & Miklossy, J. Synchrotron-based infrared and X-ray imaging shows focalized accumulation of Cu and Zn co- localized with beta-amyloid deposits in Alzheimer's disease. *J Struct Biol* **155,** 30–37 (2006).

42. Stelmashook, E., Isaev, N., Genrikhs, E., Amelkina, G., Khaspekov, L., Skrebitsky, V., & Illarioshkin, S. Role of zinc and copper ions in the pathogenetic mechanisms of Alzheimer's and Parkinson's diseases, *Biochemistry-Moscow* **79**, 391-396 (2014).

43. Bush, A. I., & Tanzi, R. E. Therapeutics for Alzheimer's disease based on the metal hypothesis, *Neurotherapeutics* **5**, 421-432 (2008).

44. Armas, A., Sonois, V., Mothes, E., Mazarguil, H., & Faller, P. Zinc(II) binds to the neuroprotective peptide humanin. *Journal of Inorganic Biochemistry* **100**, 1672-1678 (2006).

45. Wuthrich, K. Sequential individual resonance assignments in the 1H-NMR spectra of polypeptides and proteins. *Biopolymers* **22**, 131-138 (1983).
46. Keeler J. "Understanding NMR spectroscopy" 2nd edn, John Wiley & Sons, (2011).

47. Craik, D.J. & Wilce J.A. Studies of protein-ligand interactions by NMR. *Methods in molecular biology*. **60**, 195-232 (1997).

48. Fielding, L. NMR methods for the determination of protein-ligand dissociation constants. *Progress in Nuclear Magnetic resonance Spectroscopy* **51,** 219-242 (2007).

49. Van, Q. N., & Shaka, A. J. Improved cross peak detection in two-dimensional proton NMR spectra using excitation sculpting. *J Magn Reson* **132**, 154-158(1998).

50. Delaglio, F., Grzesiek, S., Vuister, G. W., Zhu, G., Pfeifer, J., & Bax, A. NMRPipe: a multidimensional spectral processing system based on UNIX pipes. *J Biomol NMR* **6**, 277-293 (1995).

51. Mallol, R., Rodríguez, M. A., Heras, M., Vinaixa, M., Plana, N., Masana, L., Morris, G. A., & Correig, X. Particle size measurement of lipoprotein fractions using diffusion-ordered NMR spectroscopy. *Anal Bioanal Chem* **402**, 2407-2415 (2012).

52. Güntert, P., Mumenthaler, C., & Wüthrich, K. Torsion angle dynamics for NMR structure calculation with the new program DYANA. *J Mol Biol* **273**, 283-298 (1997).

53. Herrmann, T., Güntert, P., & Wüthrich, K. Protein NMR structure determination with automated NOE assignment using the new software CANDID and the torsion angle dynamics algorithm DYANA. *J Mol Biol* **319**, 209-227 (2002).

54. Schwieters, C. D., Kuszewski, J. J., Tjandra, N., & Clore, G. M. The Xplor-NIH NMR molecular structure determination package. *J Magn Reson* **160**, 65-73 (2003).
55. Schwieters, C., Kuszewski, J., & Clore, G.Using Xplor-NIH for NMR molecular structure determination. *Progress in Nuclear Magnetic Resonance Spectroscopy* **48**, 47-62 (2006).

56. Laskowski, R., Rullmann, J., MacArthur, M., Kaptein, R., & Thornton, J. AQUA and PROCHECK-NMR: Programs for checking the quality of protein structures solved by NMR, *Journal of Biomolecular Nmr* **8**, 477-486 (1996).

57. Kobayashi, N. (2014) A robust method for quantitative identification of ordered cores in an ensemble of biomolecular structures by non-linear multi-dimensional scaling using inter-atomic distance variance matrix. *Journal of Biomolecular Nmr* **58**, 61-67 (2014).

58. Joosten, R., Beek, T., Krieger, E., Hekkelman, M., Hooft, R., Schneider, R., Sander, C., & Vriend, G. A series of PDB related databases for everyday needs. *Nucleic Acids Research* **39**, D411-D419 (2011).

59. Kabsch, W., & Sander, C. Dictionary of protein secondary structure: pattern recognition of hydrogen-bonded and geometrical features. **22**, 2577-2637 (1983).

60. Hashimoto, Y., Terashita, K., Niikura, T., Yamagishi, Y., Ishizaka, M., Kanekura, K., Chiba, T., Yamada, M., Kita, Y., Aiso, S., Matsuoka, M., & Nishimoto, I. Humanin antagonists: mutants that interfere with dimerization inhibit neuroprotection by Humanin. *Eur J Neurosci* **19**, 2356-2364 (2004).

61. M. Maftei, X. Tian, M. Manea, et al, Interaction structure of the complex between neuroprotective factor humanin and Alzheimer's β-amyloid peptide revealed by affinity mass spectrometry and molecular modeling, J. Pept. Sci. 18 (2012) 373–382.

62. Maret, W. New perspectives of zinc coordination environments in proteins. *Journal of Inorganic Biochemistry* **111**, 110-116 (2012).

63. Maret, W. Zinc and sulfur: A critical biological partnership. *Biochemistry* **43**, 3301-3309 (2004).

64. Laaksamo, E., Tulamo, R., Liiman, A., Baumann, M., Friedlander, R., Hernesniemi, J., Kangasniemi, M., Niemela, M., Laakso, A., & Frosen, J. Oxidative Stress Is Associated With Cell Death, Wall Degradation, and Increased Risk of Rupture of the Intracranial Aneurysm Wall. *Neurosurgery* **72**, 109-117 (2013).

65. Smith, D., Cappai, R., & Barnham, K. The redox chemistry of the Alzheimer's disease amyloid beta peptide. *Biochimica et Biophysica Acta-Biomembranes* **1768**, 1976-1990 (2007).

66. Cuajungco, M., Goldstein, L., Nunomura, A., Smith, M., Lim, J., Atwood, C., Huang, X., Farrag, Y., Perry, G., & Bush, A. Evidence that the beta-amyloid plaques of Alzheimer's disease represent the redox-silencing and entombment of A beta by zinc. *Journal of Biological Chemistry* **275**, 19439-19442 (2000).

67. Arakawa, T., Kita, Y., & Niikura, T. A rescue factor for Alzheimer's diseases: discovery, activity, structure, and mechanism. *Curr Med Chem* **15,** 2086–2098 (2008).

Solution NMR studies of CERT-PH domain interaction with phospholipid bilayers in nanodiscs as a model membrane system

1 Introduction

1.1 Lipid transport by lipid transfer proteins

Eukaryotic cells are structurally complex and organized into smaller compartments (organelles) and each organelle had a specific functions and specific lipid and protein composition [1]. The allocation of the proteins among the cellular organelles is predominantly regulated and mediated by specific protein-targeting molecules and can be regulated by the chemical modifications and the conformational changes. Lipids lack any specific intrinsic motifs to mediate their distribution inside the cell; but it is still, there is a large variation on the lipid composition of membranes in the cell [2, 3]. The lipid synthesis and sorting are extremely important for the biogenesis of membranes and for the lipid mediated signaling pathways inside the cell. A number of studies suggest that the lipid trafficking inside the cell from the site of the synthesis in the endoplasmic reticulum (ER) to the different target membranes is mediated by both vesicular transport and non-vesicular transport mechanisms [4]. The major lipid transport mechanism inside the cell is the Non-vesicular lipid transport. Lipids can be transported non-vesicular way by spontaneous lipid transport or by lipid transfer proteins (LTP).

Lipid Transfer Proteins (LTPs)

Lipid transfer proteins are intracellular proteins that can transfer the lipid molecule by attaching it to a hydrophobic pocket in the protein and transfer it between membranes.

At first, it was discovered as a soluble factors that act in acceleration of the exchange or the net transfer of different lipid molecules between different membranes in vitro [6]. Afterward, many LPTs have been discovered and studied and many crystal structures have been resolved. The mode of action of LTPs have not been fully explored even though they have been extensively studied for a long time. LTPs can locally regulate and modify the lipid composition of membranes thereby controls various cellular processes including vesicular trafficking, lipid metabolism and signal transduction [5]. LTPs can be specific to one or two type of lipid and it can contain a single structural lipid transfer domain or can have more additional structural domains with specific functions [7].

1.2 Ceramide Trafficking Protein (CERT)

In the mammalian cells, ceramide is synthesized in in the endoplasmic reticulum (ER) and then transported by CERT to the Golgi complex, to be used in the synthesis of the sphingomyelins (SM). CERT has a two membrane targeting parts; the PH domain which bind PtdIns4P (PI4P) specifically and mediates CERT binding to the Golgi complex, and the FFAT motif which interacts with the ER membrane protein VAP, thereby mediate the binding to the ER membrane [8,fig.19]. Mutations in the CERT PH domain abolish its Golgi targeting and, consequently, the synthesis of sphingomyelin lipids.

CERT consists of three parts [fig. 18]. The amino terminal region (about 120 amino acid residues), forms the pleckstrin homology (PH) domain that responsible for the Golgi targetting. The carboxyl terminal region (about 230 amino acid residues) forms a START domain responsible for extracting the ceramide molecule from membranes of ER and

transfer the bound ceramide to Golgi membranes. The middle region form no globular domains, has a short peptide motif FFAT interacts with the ER membrane protein VAP [9, 10]. PH and START domains are both needed for the efficient ceramide transfer by CERT [8.11]. The direction of the transfer and final destination of ceramide molecule is controlled by the PH domain through its specific binding to phosphatidylinositol 4-monophosphate (PI4P), a phosphoinositide that is mainly associated to the Golgi membranes.

1.2.1 Structure of CERT PH domain:

Solution structure and Crystal structure of CERT PH domain have been determined previously [12, 13]. The CERT PH domain structure shows a characteristic seven β-strands (β1 – β7) and one C-terminal α-helix [12, figure 20A]. The core structure forms a β-sandwich structure that is closely packed, and the C-terminal α-helix lies on the top of the β-sandwich. The structure shows a basic groove (basic amino acid residues) that runs along the middle of the protein [figure 20 B].

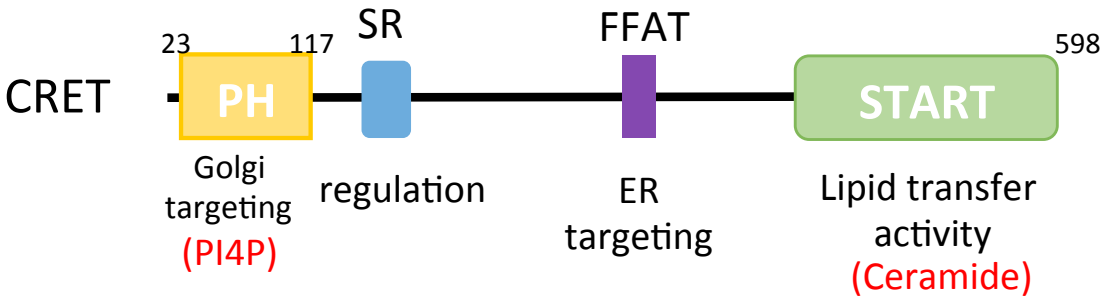

Figure 18. Structure of CERT. PH domanin function in Golgi targeting, the middle region function in interaction with ER and regulation of CERT function by regulation, and the START domain responsible of inter-membrant transfer of ceramide.

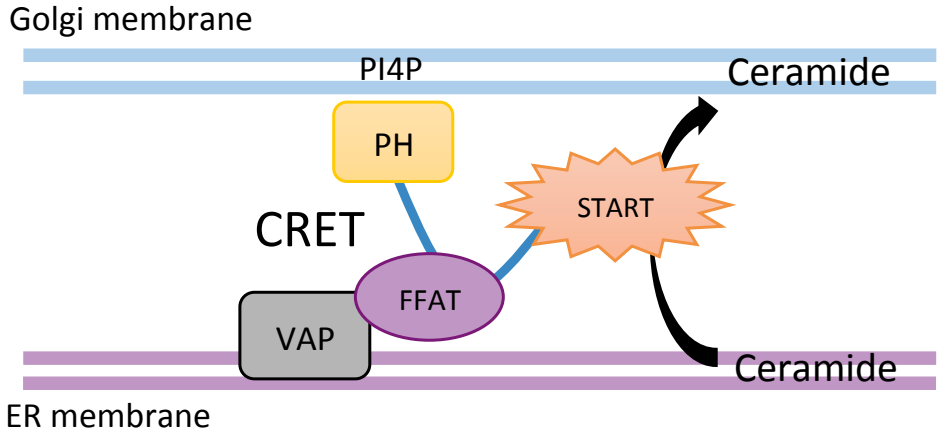

Figure 19. Proposed model of CERT –mediated trafficking of ceramide at the ER-Golgi contact sites.

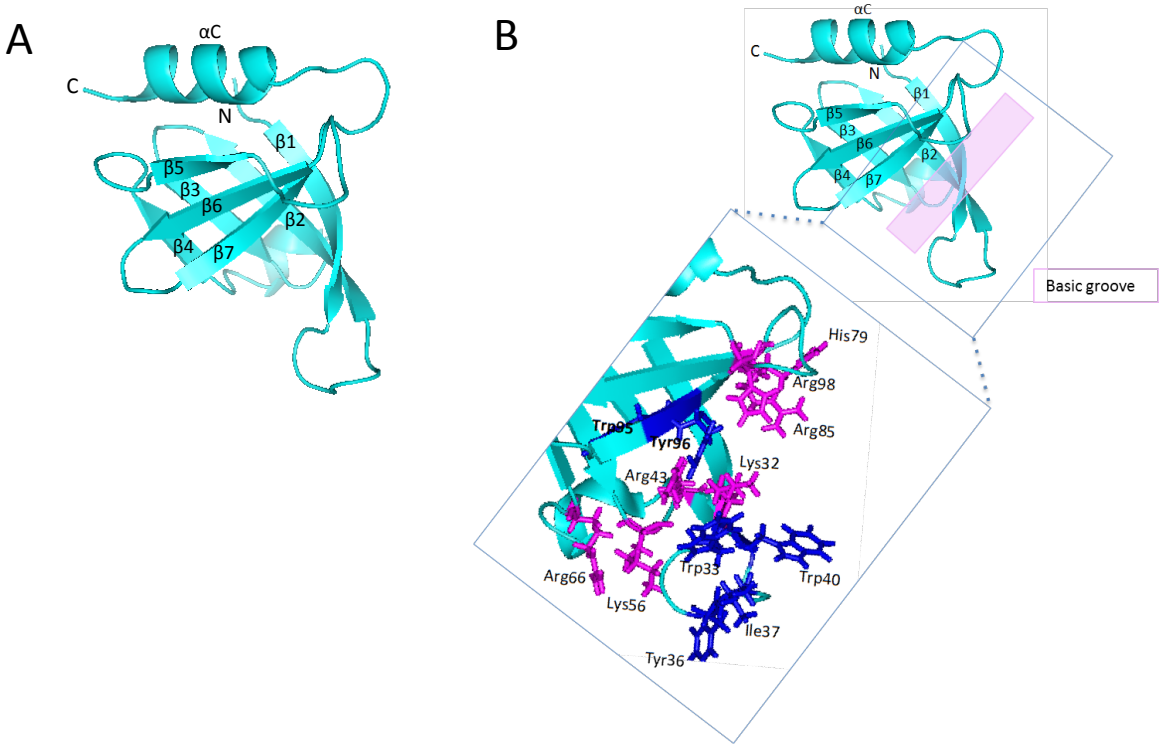

Figure 20. Solution structure of CERT PH domain. A) A ribbon representation of the solution structure of PH domain (PDB; 2RSG). B) Representation of the PH domain structure showing the position of the basic groove (basic amino acid residues) [12].

1.3 Phospholipid bilayer Nanodisc

Nanodisc is a model membrane system that has been developed by Sliger et al. [14, 15], a self–assembled discoidal phospholipid bilayers surrounded and stabilized by two membrane scaffold protein (MSP) molecules, as illustrated in figure 20. Each nanodisc is composed by a certain number of phospholipids in the form of a phospholipid bilayer. Two MSPs surround the bilayer shielding the hydrophobic alkyl chains of the phospholipids from the aqueous environment, thereby creating a soluble nanoscale lipid bilayer. Nanodiscs assemble by adding amphipathic membrane scaffold protein (MSP) to detergent solubilized phospholipid in a suitable molar ratio. The nanodisc self-assembles upon removal of the detergent by dialysis or by binding to beads for detergent removal. The phospholipid to MSP molar ratio is important and the length of MSP determines the diameter of the disc.

The ApoA-1 derivatives used as MSPs for the nanodiscs introduced by Sliger and co-workers. MSPs are created by genetic engineering of the ApoA-1 encoding sequence. Two-copies of MSP warp around the phospholipid bilayer and defines the diameter of disc and create a uniformly size water soluble nanoscale bilayers. The stoichiometric ratio between lipids and MSP needs to be controlled to produce monodisperse discs. This ratio is different for different lipids. And the temperature should also be controlled during assembly [14].

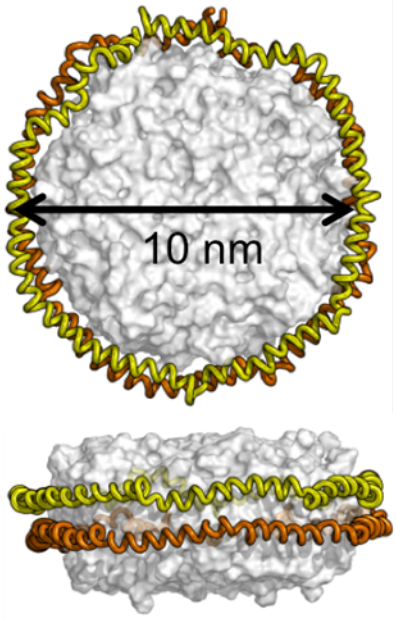

Figure 21. Nanodisc; a discoidal phospholipid bilayer encircled by 2 copies of MSP measuring ≈10 nm in diameter

1.4 Study of protein lipid binging using ITC

Isothermal titration colorimetry (ITC) is a physical technique that is used to study the thermodynamics of the interaction between two molecules. It can determine the thermodynamic parameters and directly quantify the K_d values without the need to use of any label. It used for the characterization of molecular interactions between proteins, lipids, antibodies, sugars, etc. and any small ligands.

In a typical experiment aliquots of a titrant molecule (ligand), placed in the syringe, are injected into the biomolecule solution, and placed in the sample cell. The amount of heat that generated or absorbed upon each titration due to the interaction of molecules, proportional to complex that formed, is measured and this energy used to for the determination of the equilibrium dissociation constant (Kd), the binding enthalpy (ΔH), and

the number of binding sites or stoichiometry (n). We can calculate the Gibb's free energy ΔG and entropy ΔS [16]. The thermodynamic measurement can provide information about the nature of the forces that responsible of the binding between the molecules in addition to the conformation of the direct interaction.

One important application of the ITC is the drug discovery. ITC is one of the recent techniques to be used to characterize the affinity of the binding of ligands for proteins. ITC is especially useful because it gives the binding affinity and also the thermodynamics of the binding it provides a complete thermodynamic profile in a just one experiment. This thermodynamic characterization by ITC allows for more optimization of the compounds [17].

2 Experimental

2.1 Expression and purification of CERT PH domain

The Human CERT PH domain (residues 23-117) was prepared. The DNA fragments encoding amino acid residues was amplified by PCR, cloned onto pET28a plasmid (Navogen) and expressed at 25°C in *E.coli* BL21 (DE3) strain with His-tag at the N terminus followed by HRV3C protease recognition site. The uniformly ^{15}N-labeled CERT PH domain were prepared by growing *E.coli* host in M9 minimal media containing [^{15}N] ammonium chloride.

The His6-tagged CERT PH domain was purified by metal-chelating chromatography, using Ni-NTA affinity column (QIAGEN Ni-NTA resin). The His6 tag was then removed from the purified protein by enzymatic digestion with tobacco etch virus protease (Invitrogen). The CERT PH domain was further purified by gel filtration. The protein fractions loaded onto HiLoad 16/60 Superdex200 pg column (GE Healthcare) using Acta Prime Plus (GE Healthcare) and the fractions containing the protein were eluted and the purity checked by SDS-PAGE.

2.2 Preparation of Nanodisc

Expression and purification of MSPI D1

Purified plasmid DNA of MSP1 cloned into pET28a plasmid as a fusion protein with GB1 and His-tag was transformed into *E. coli* strain BL21 (DE3) and expressed at 28°C. The His6-tagged MSP1D1 was purified by metal-chelating chromatography, using Ni-NTA affinity column (QIAGEN Ni-NTA resin). The His6 tag was then removed from the purified protein by enzymatic digestion with tobacco etch virus protease (Invitrogen). The

MSP1D1 was further purified by gel filtration. The protein fractions loaded onto HiLoad 16/60 Superdex200 pg column (GE Healthcare) using Acta Prime Plus (GE Healthcare) and the fractions containing the protein were eluted and the purity checked by SDS-PAGE.

Nanodisc reconstitution

The 1,2-dioleoyl-sn-glycero-3-phosphocholine (DOPC) and 1,2-dioleoyl-*sn*-glycero-3-phospho-(1'-myo-inositol-4'-phosphate) (PI(4)P) were purchased from Avanti Polar Lipids, inc. PI4P was solved in a mixed solvent (chloroform: Methanol: water = 1:2:0.8 in volume ratio). PI4P mixed with DOPC, and the solvent dried under stream of nitrogen gas and farther placed in vacuum desiccator overnight. Lipid film solubilized in dterergent and mixed with MSP1D1 (optimal MSP1D1: lipid ration was determined to be 1:60) and the mixture incubated. Then Bio-beads were used to remove the detergent and in the final step nanodisc was purified by gel filtration.

2.3 NMR measurements

All the NMR experiments for CERT PH domain were carried out at 25°C on a Bruker 500 MHz equipped with BBO Cryoprobe. The spectra measured with a protein concentration of 0.1-0.2 mM in a buffer solution consists of 10 mM HEPES-NaOH buffer (pH 7.5), containing 100 mM NaCl and 2 mM DTT in 90% H_2O/10% D_2O.

^{31}P NMR experiments were carried out at 25°C on Bruker 500 MHz with BBO Cryoprobe. The buffer solution consists of 20mM Tris-HCl (pH 7.4) and 100mM NaCl in 90% H_2O/10% D_2O. For the NMR measurement, the concentration of nanodisc was 80uM used both with and without PI4P. All of the 2D NMR spectra were processed and analyze

by programs NMRPipe [50] and Sparky (T. D. Goddard and D. G. Kneller, SPARKY 3, University of California, San Francisco), respectively.

2.4 ITC experiments

Isothermal titration were performed with VP-ITC at 25°C. In individual titrations, 12 μM injection of ligand stock (200 μM CERT PH domain) was injected (20 times in total) with initial delay 1400 sec and spacing time of 600 sec in to the nanodisc solution (15 μM). The buffer was HEPES-NaOH buffer (pH 7.5) containing 100 mM NaCl and 2mM DTT.

3 Results and discussion

3.1 CERT PH binding to PI4P-containing nanodisc

To identify the CERT PH domain binding to phospholipid bilayer nanodisc, nanodisc samples containing PI4P lipids were prepared and ^{1}H-^{15}N HSQC spectra for uniformly ^{15}N-labeled CERT PH apo form and interacting with nanodisc were measured. Figure 22 shows the preparation of CERT PH domain conjugated to nanodisc (figure 22B). ^{1}H-^{15}N HSQC spectra for CERT PH apo form and CERT PH conjugated to nanodisc were measured and compared and NMR signals of the bound state CERT PH could be detected (figure 22 B).

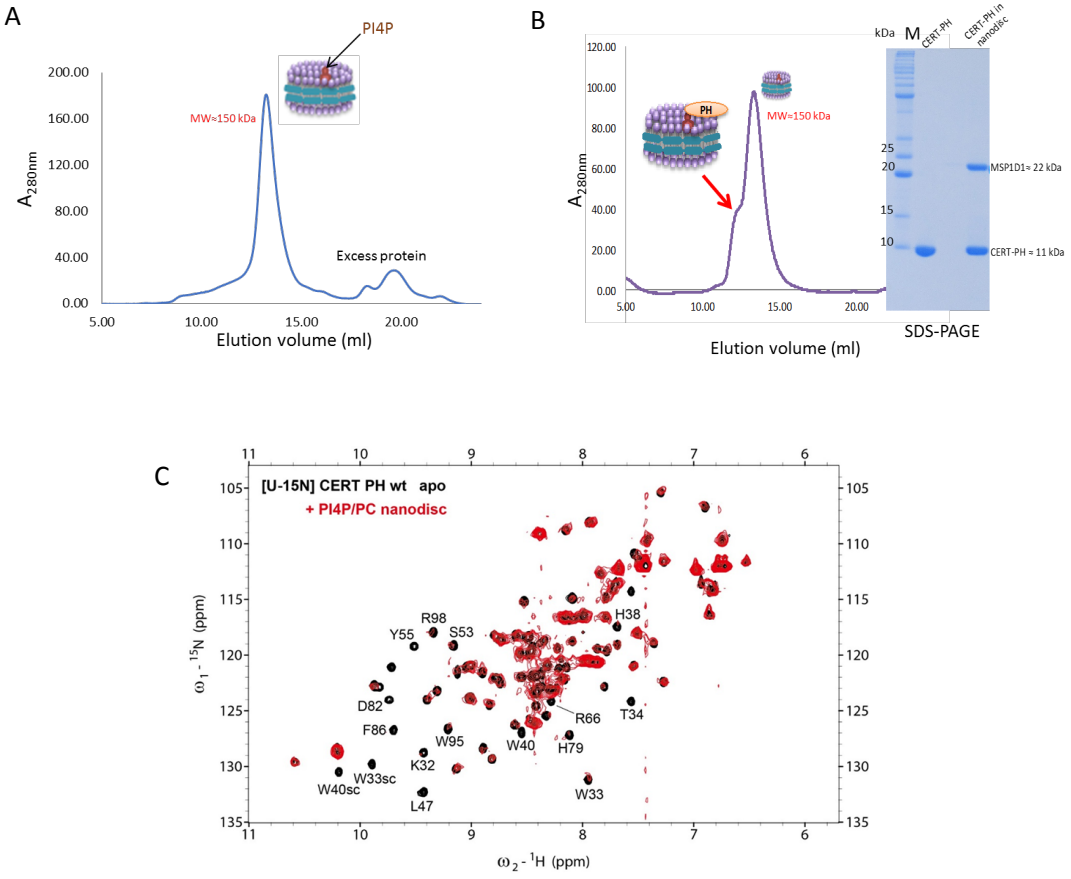

Figure 22: Interaction of CERT PH domain with PI4P-contaiong nanodisc. A) Superdex 200 chromatogram of PI4P-containing nanodisc. B) Superdex 200 chromatogram of PI4P-containing nanodisc afterconjugation with CERT PH. C) ^{15}N HSQC spectra of uniformly labeled 0.1 mM free (Black) CERT PH and CERT PH conjugated to nanodisc (red) in molar artio (1:0.5).

Bicelles, liposomes and nanodiscs are commonly used for functional analysis as a membrane mimetics. Among these methods, nanodisc is the suitable choice to be used as a tool for analyzing membrane protein interaction in solution. The other systems have some disadvantages; liposomes are large and insoluble in water and bicelles contains detergents which may be harmful for the protein. And also nanodisc can be easily quantified, based on the absorbance at 280nm of MSP and this is extra advantage of using nanodisc in quantitative analysis.

3.2 Membrane binding site on CERT PH domain

To identify the membrane binding site on the CERT PH domain, we performed chemical shift perturbation (CSP) experiments. ^{15}N HSQC spectra of CERT PH domain interacting with 2% PI4P containing nanodisc reveals the shifting of certain amid peaks (fig23). Residues (Trp-40, Trp-33, Asn-35, Trp-95) and the side chain of (Trp-40, Trp-33) exhibited considerable chemical shift changes (figure 23, 24). The results indicated that the binding affects several amino acid residues and those residue that show significant shift changes are directly involved in the binding of PH domain to the membrane.

From this result we suggested that a hydrophobic force that derives CERT PH domain to the lipid head groups and the basic amino acid residues in the basic groove of CERT PH domain (figure 20) mainly contribute to the lipid membrane interaction. And this results are consistent with a previous study using liposomes as model membrane to study CERT PH interaction [12].

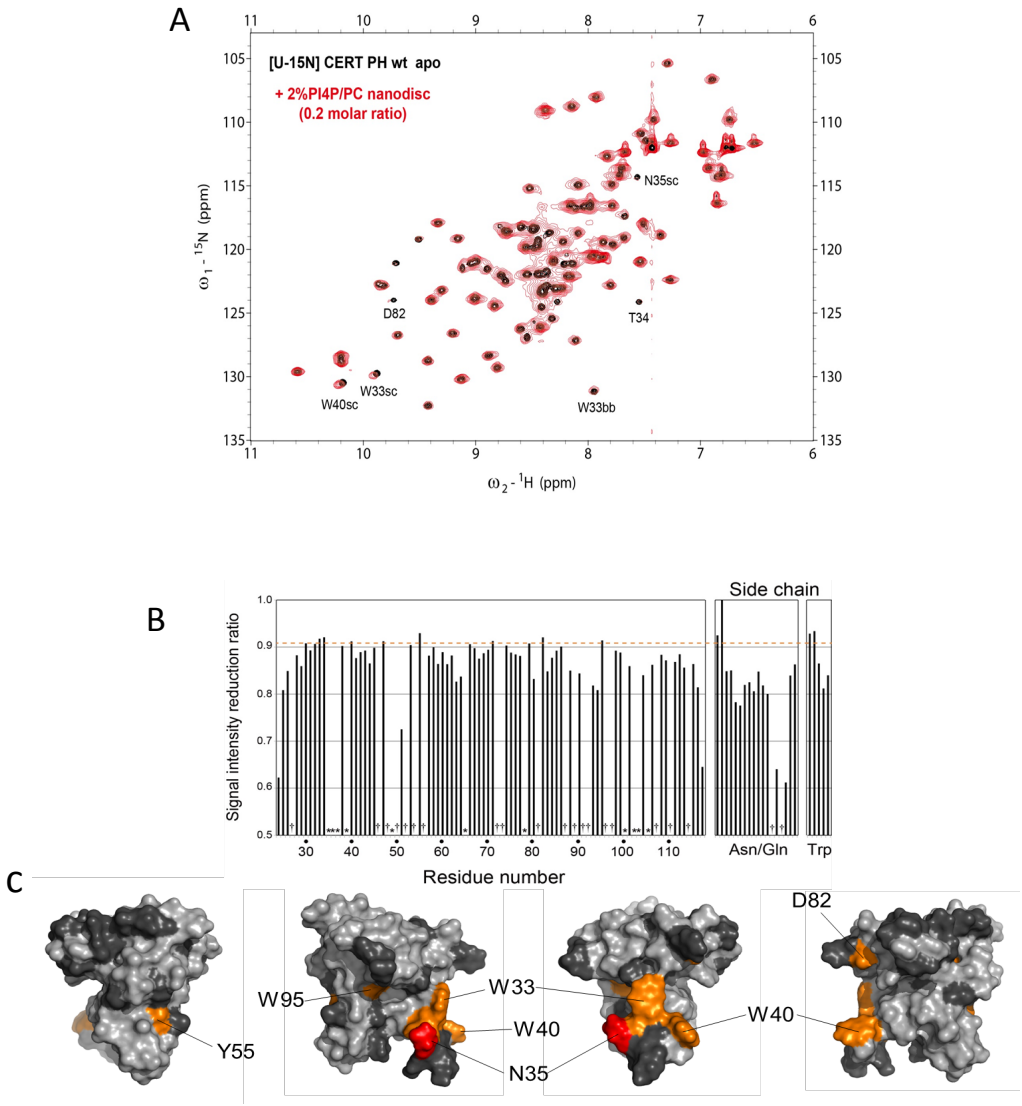

Figure 23. Identification of membrane binding site on CERT PH domain. A) ^{15}N HSQC spectra of uniformly^{15}N- labeled 0.1 mM free (Black) CERT PH and CERT PH conjugated to nanodisc containing 2% PI4P (red) in molar rartio (1:0.2). B) A plot shows the signal intensity reduction ratio of CERT PH domain residues due to the binding to PI4P nanodisc .C) Mapping of the residues that were show significant intensity reduction upon the binding with nanodisc (red and orange).

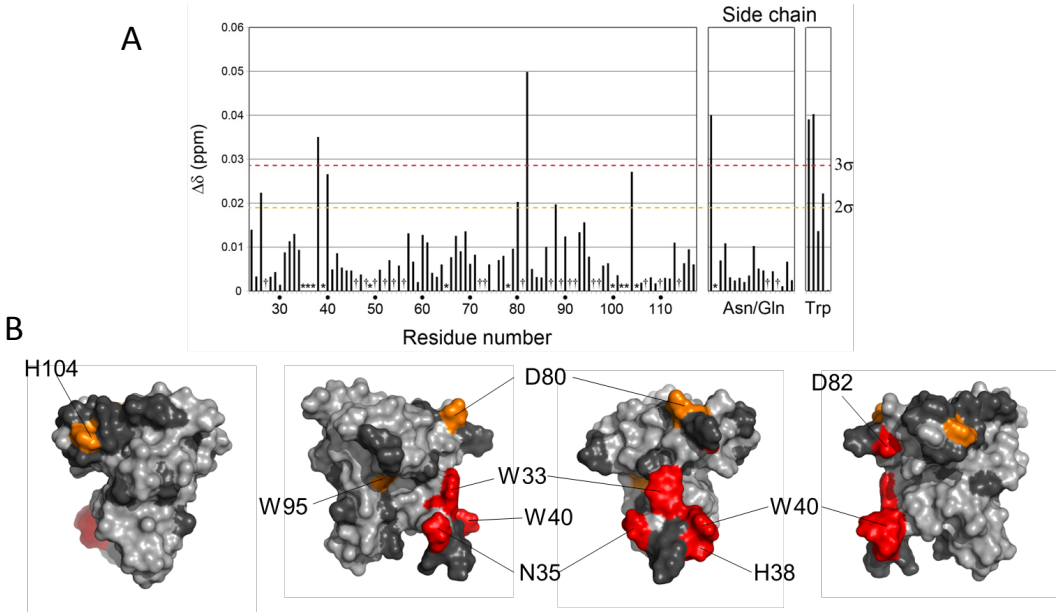

Figure 24. A) Normalized chemical shift changes of individual residues in the CERT PH domain due to the binding to nanodisc. B) Mapping of the residues that were significantly perturbed by the interaction with the membrane bilayer nanodisc (Red and orange).

Many experimental and theoretical work has proved in spite of the fact that nonspecific interactions may not be enough to anchor peripheral proteins at the surface of the membrane , these nonspecific interactions are necessary for the membrane targeting and for the biological functions of the proteins [18]. The specific interactions of proteins with lipid ligands are facilitated with the initial nonspecific interaction of proteins with membranes. The initial nonspecific attachment of the protein to the membrane can also support the penetration of the hydrophobic and aromatic residues on the surface of the proteins into superficial region in the lipid bilayer [18].

3.3 Characterization of CERT PH domain binding to lipid bilayer with ITC

In order to characterize the binding of CERT PH domain to the lipid bilayer nanodisc, the interaction was monitored by means of ITC. Titration of CERT PH domain

with PC only nanodisc and P14P/PC nanodisc were performed. The titration experiments were performed at 25°C with the sample, nanodisc (15 uM) in the titration cell.

At first, PI4P-containing nanodisc titrated with CERT PH domain and the result show that a large exothermic reactions were observed (figure 25A). The interaction had a k_d = 0.152 μM, ΔH =-19.4 kcal/mol, -TΔS=10.1 kcal/mol and ΔG= -9.3 kcal/mol. the result indicated that CERT PH domain binds to PI4P-containing nanodisc with a strong binding affinity and one to one binding stoichiometry.

Further, PC only nanodisc titrated with CERT PH domain and the result is shown in figure 25B, there is no marked heat of binding reaction. This indicated a very weak interaction between the CERT PH domain and the PC nanodisc. These findings indicated that in PI4P is necessary for the binding of CERT to the membrane.

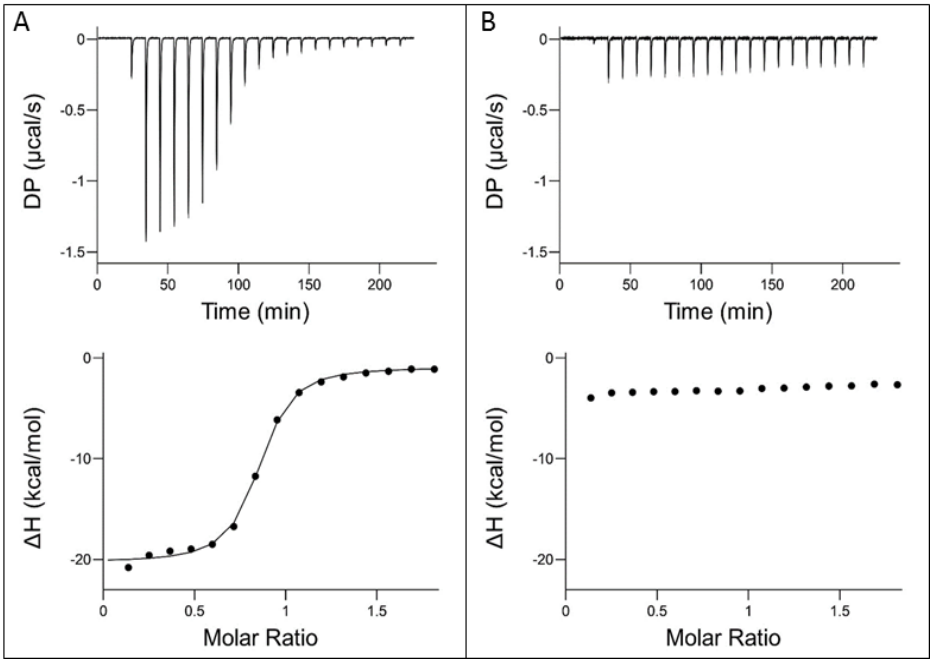

Figure 22. ITC experiment following nanodisc binding to CERT PH domain. A) PC/PI4P-containing nanodisc binding to CERT PH domain. B) PC only nanodisc binding to CERT PH domain.

4. Conclusions

Nanodisc can be used for structural analysis of the interaction between Protein and membrane by solution NMR using CSP analysis which is powerful in distinguishing between the residue involve in the direct binding and conformational changes under nearly physiological condition, without chemical modification on the protein. Nanodisc could be applied to study thermodynamic of the interaction between membrane protein and lipid by layer using ITC.

In this study, Phospholipid bilayer Nanodisc containing a functional lipid ligand (PI4P) were prepared and used in structural-functional studies of membrane protein CERT, using solution NMR technique (CSP). Residues involved in the direct binding of CERT PH domain with membrane by layer could be determined. NMR showed that Trp residues in CERT-PH interacted with the membrane. The neighboring basic 4 Arg and 2 Lys residues should interact specifically with the anionic head group of PI4P. CERT-PH should target the Golgi body by the electrostatic protein-PI4P interaction for membrane trafficking.

ITC technology was applied to study the membrane protein CERT interaction with the lipid bilayer. ITC showed a strong binding affinity (Kd = 0.15 μM) between CERT-PH and PI4P nanodisc with stoichiometry 1:1. The result suggested that PI4P enhances the binding affinity of CERT PH-domain to the membrane.

References

1. Holthuis, J. C., van Meer, G. & Huitema, K. Lipid microdomains, lipid translocation and the organization of intracellular membrane transport (Review). *Mol. Membr. Biol*. **20**, 231–241 (2003).

2. Sprong, H., van der Sluijs, P. & van Meer, G. How proteins move lipids and lipids move proteins. *Nature Rev. Mol. Cell Biol*. **2**, 504–513 (2001).

3. Voelker, D. R. Organelle biogenesis and intracellular lipid transport in eukaryotes. *Microbiol. Rev*. **55**, 543–560 (1991).

4. Voelker, D. R. lipid transport pathways in mammalian cells. *Experientia* **46**,569-579.

5. Lev, S. Non-vesicular lipid transport by lipid-transfer proteins and beyond. Nat Rev *Mol Cell Biol.***11**, 739-50 (2010).

6. Wirtz, K.W. & Zilversmit, D. B. Exchange of phospholipids between liver mitochondria and microsomes in vitro. *J Biol Chem* **243**, 3596–3602 (1968).

7. D'Angelo, G., Vicinanza, M. & De Matteis, M. A. Lipid–transfer proteins in biothynthetic pathways. *Curr Opin Cell Biol*. **20**, 360-70 (2008).

8. Hanada, K. Discovery of the molecular machinery CERT for endolasmic reticulum –to-Golgi trafficking of ceramide. *Mol Cell Biochem* **286**, 23-31 (2006).

9. Hanada, K., Kumagai, K., Yasuda, S., Miura, Y., Kawano, M., Fukasawa, M. & Nishijima, M. Molecular machinery for non-vesicular trafficking of ceramide *Nature* **426**, 803-809 (2003).

10. Kudo, N., Kumagai, K., Tomishige, N., Yamaji, T., Wakatsuki, S., Nishijima, M., Hanada, K. & Kato, R. Structural basis for specific lipid recognition by CERT responsible for nonvesicular trafficking of ceramide. *Proc Natl Acad Sci U S A*. **15**, 488-93 (2008).

11. Kawano, M., Kumagai, K., Nishijima, M. & Hanada, K. Efficient trafficking of ceramide from the endoplasmic reticulum to the Golgi apparatus requires a VAMP-associated protein-interacting FFAT motif of CERT. *J Biol Chem* **281,** 30279–30288 (2006).

12. Sugiki, T., Takeuchi. K., Yamaji, T., Takano, T., Tokunaga, Y., Kumagai, K., Hanada, K., Takahashi, H. & Shimada, I. Structural basis for the Golgi association by the pleckstrin homology domain of the ceramide trafficking protein (CERT). *J Biol Chem*. **287**, 33706-18 (2012).

13. Prashek, J., Truong, T. & Yao, X. Crystal structure of the pleckstrin homology domain from the ceramide transfer protein: implications for conformational change upon ligand binding. *PLoS One* **8,** e79590 (2013).

14. Bayburt, T. H., Grinkova, Y. V. & Sligar, S. G. Self-assembly of discoidal phospholipid bilayer nanoparticles with membrane scaffold proteins. *Nano Letters* **2**, 853-856 (2002).

15. Denisov, I. G., Grinkova, Y. V., Lazarides, A. A. & Sligar, S. G. Directed Self-Assembly of Monodisperse Phospholipid Bilayer Nanodiscs with Controlled Size. *J. Am. Chem. Soc.* **126**, 3477-3487 (2004).

16. Freyer, M. W. & Lewis, E. A. Isothermal titration calorimetry: Experimental design, data analysis, and probing macromolecule/ligand binding and kinetic interactions. *Methods Cell Biol*. **84**, 79–113 (2008).

17. Ward, W. H. & Holdgate, G. A. Isothermal titration calorimetry in drug discovery. *Prog Med Chem* **38**, 309-76 (2001).

18. Cho, W. & Stahelin, R. V. Membrane-protein interactions in cell signaling and membrane trafficking. *Annu Rev Biophys Biomol Struct.* **34**,119-51(2005).

ACKNOWLEDGMENTS

I would like to express my sincere gratitude to Professor Toshimichi Fujiwara for giving me the opportunity to become a member of his lab and to do my research at the Laboratory of Molecular Biophysics at the Institute for Protein Research and for all the guidance and support.

I have worked under the guidance of Prof. Chojiro Kojima and I wish to thank him whole-heartedly for taking me into his group, I very much appreciate for his guidance and support throughout my study and for his timely advices, frequent work discussions and all scientific conversations. I thank you; it has been a real pleasure to work with you.

I acknowledge Dr. Toshihiko Sugiki for his kind help and assist with the NMR experiments and for introducing me to many amazing technique with his ample knowledge and skills.

Thanks to Ms. Yoneyama to provide and teach me the most important techniques and for her kind help on everything in the lab. My thanks also go to all the members of Kojima group for help with experiments. Thanks to all the members of Fujiwara lab for making a very friendly working environment.

Also I would like to thank Dr. Masamoto So and professor Young-Ho Lee for their assist on the CD and ITC experiments.

Thanks to all my friends for being with me through the hard times. I am forever appreciated my parents, brothers, sister for their support and unlimited love.

I dedicate this work to my family who gave me their unconditional support during these five years abroad.

Appendix

Appendix1. CD spectra of Aβ40 in the presence and absence of HNs

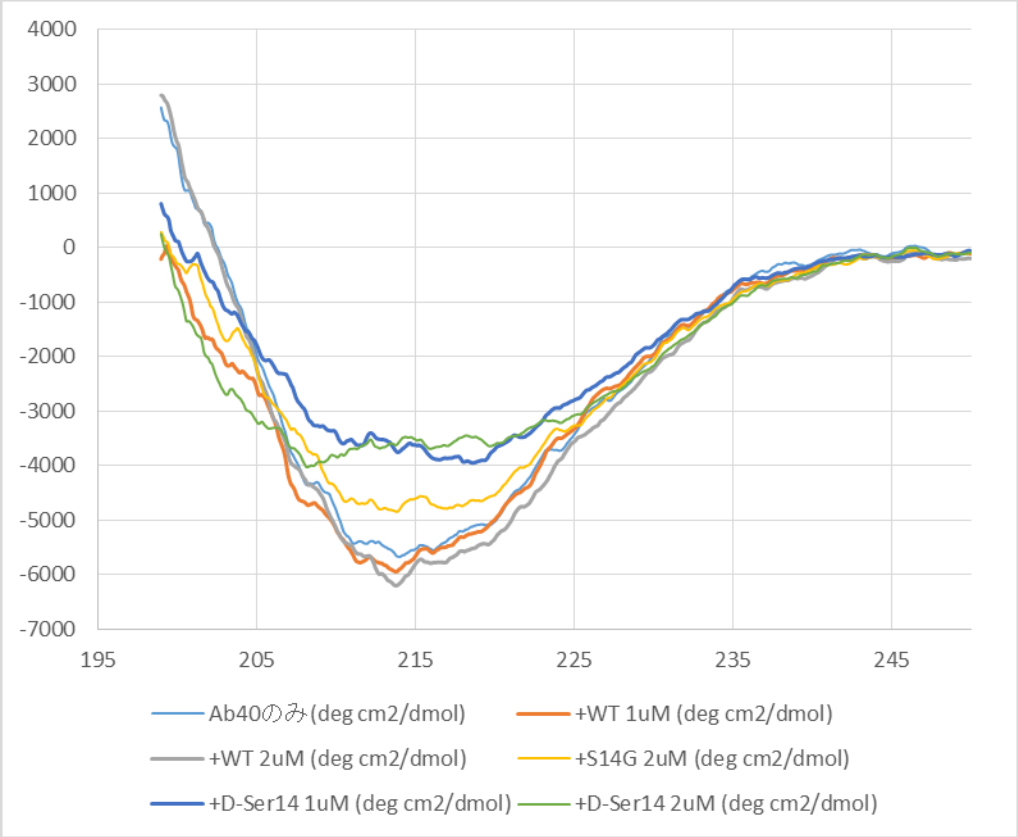

Appendix 2. Proton chemical shifts of the HN D-Ser14

Table 1. Proton chemical shifts (ppm) of the HN D-Ser14

Residue	HN	αCH	βCH	Others
Met1		4.116	2.164	γCH2: 2.633
				εCH3: 2.110
Ala2	8.495	4.646	1.375	
Pro3		4.445	2.308	γCH2: 1.957
				δCH2: 3.563/3.783
Arg4	8.303	4.298	1.843	γCH2: 1.729/1.674
				δCH2: 3.224
				εNH: 7.174
				NH2: D[†]
Gly5	8.369	4.024/3.873		
Phe6	8.052	4.418	3.908/3.164	δCH2(2,6H): 7.181
				εCH2(3,5H): 7.277
				ζCH(4H): –[‡]
Ser7	7.998	4.089	3.974/3.881	
Cys8	7.889	4.160	2.983	
Leu9	7.725	4.079	1.718	γCH: 1.647
				δCH3: 0.9110/0.8550
Leu10	7.807	3.855	1.271/1.843	γCH: 1.505
				δCH3: 0.7130/0.7850
Leu11	7.582	4.081	1.769/1.835	γCH: −
				δCH3: 0.9120
Leu12	8.447	4.125	1.624	γCH: 1.872
				δCH3: D
Thr13	7.783	4.300	4.456	γCH3: 1.327
Ser14	7.702	4.313	4.106	

Glu15	8.136	4.340	2.264/1.910	γCH2: 2.463/2.437
Ile16	7.452	4.093	1.732	γCH2: 1.156
				γCH3: 0.8560
				δCH3: 1.366
Asp17	7.947	4.792	2.925/2.755	
Leu18	7.760	4.532	1.715	γCH: 1.531
				δCH3: 0.9480/0.9140
Pro19		4.458	2.229	γCH2: 2.026
				δCH2: 3.628/3.800
Val20	7.511	4.060	2.112	γCH3: 0.9410
Lys21	8.032	4.304	1.792/1.864	γCH2: 1.434/1.491
				δCH2: 1.705
				εCH2: 3.000
				εNH3: 7.613
Arg22	8.080	D	D	D
Arg23	8.095	D	D	D
Ala24	8.095	4.293	1.414	

[‡]"D" denotes that signals were detected but could not be assigned because of degeneracy of the signals

[†]"–" denotes absence of the corresponding signals

Appendix 3.

^{15}N-HSQC experiments for CERT PH domain interaction with 5%PI4P-containing nanodisc

(a) ^{1}H-^{15}N HSQC Overlay (all) CERT PH (blue)+ CERT PH + 5%PI4P ND (blue)

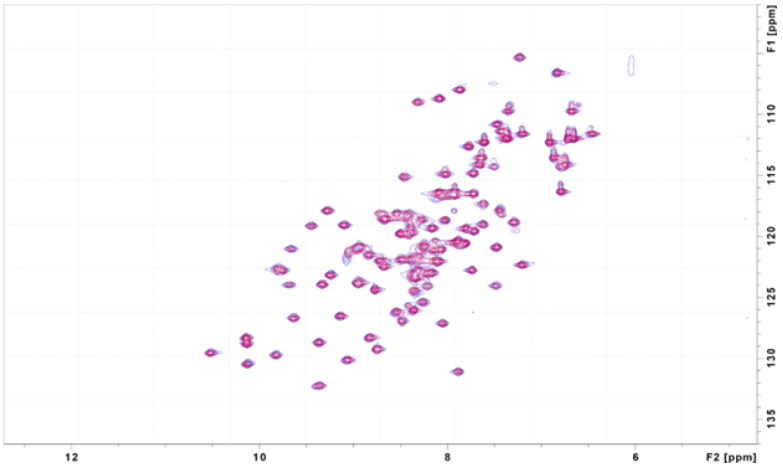

(b) ^{1}H-^{15}N HSQC (all) overlay of CERT PH + 5%PI4P ND, Thr34.

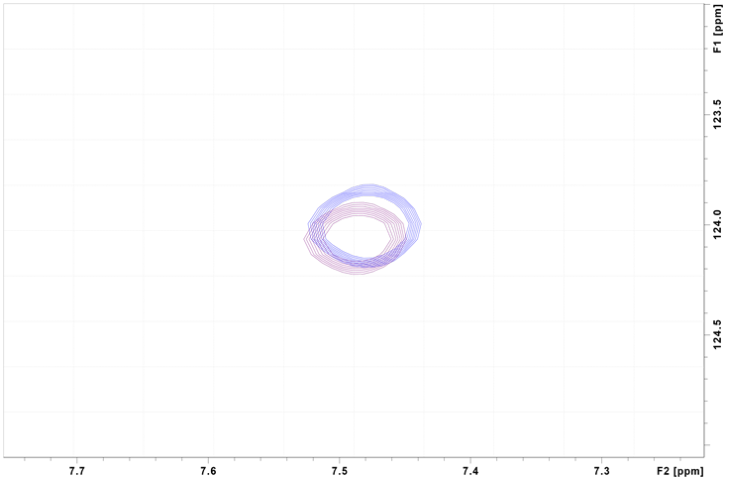

(c)Overlay of CERT PH Apo+ 5%PI4P ND(All)

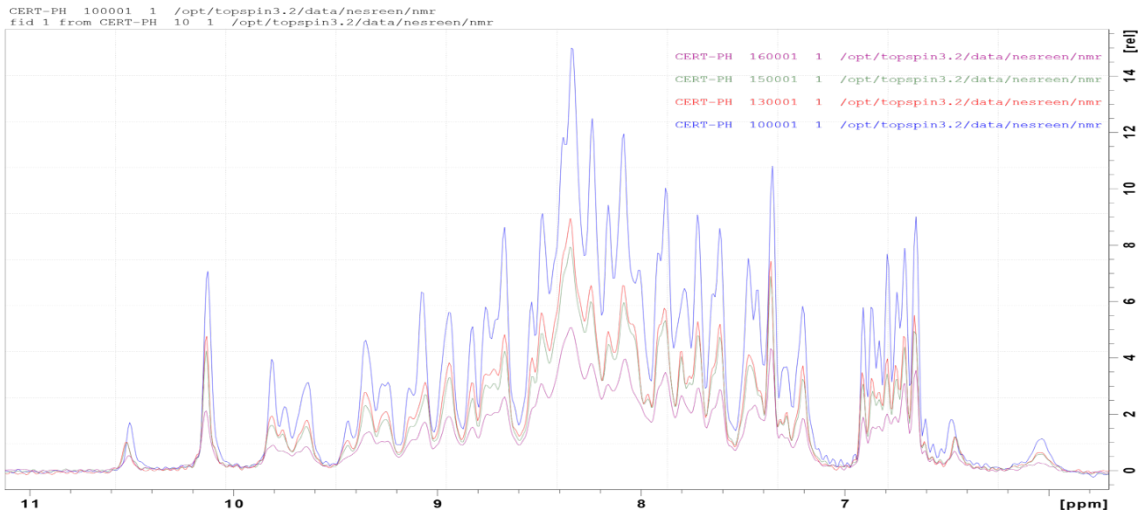

(d)^{15}N HSQC Overlay (all) CERT PH Apo+ 5%PI4P ND, Trp(sc)